Final report on AN/MPQ-501 receiver improvement work

Hendry, A.

Report (National Research Council of Canada. Radio and Electrical Engineering Division : ERB), 1967-01

ERB-759

CONFIDENTIAL

COPY NO.

NATIONAL RESEARCH COUNCIL OF CANADA

RADIO AND ELECTRICAL ENGINEERING DIVISION

FINAL REPORT
ON AN/MPQ-501 RECEIVER IMPROVEMENT WORK

A. HENDRY

OTTAWA

JANUARY 1967 NRC # 35685

ABSTRACT

Recent work on improvement of the AN/MPQ-501 counter mortar radar receiving system is summarized, along with calculated and measured effects of rainfall on the system. Laboratory evaluation of an image-rejection mixer and a commercial parametric amplifier indicates that a basic receiver noise figure close to 4 db can be obtained. A revision of the noise monitor equipment to improve its accuracy is described. The construction and performance of a ceramic waveguide window having a VSWR less than 1.1 within the radar band is included. Measurement of the effectiveness of the circular polarizer as a means of reducing rain clutter indicates a gross cancellation of about 20 db. Measured clutter levels of 22 to 32 db above receiver noise power for light to moderate rainfall rates at a range of 10 km are reported.

TABLE OF CONTENTS

Confidential

FIGURES

PLATES

FINAL REPORT ON AN/MPQ-501 RECEIVER IMPROVEMENT WORK

- A. Hendry -

1. RECEIVER SENSITIVITY IMPROVEMENT

1.1 Introduction

The advent of practical low-noise amplifiers for Ku-band provides the means for greatly improving the sensitivity of the receiver. Until relatively recently, the only amplifiers available for the 16-GHz band were traveling-wave tube amplifiers (TWT's) which, at best, could not provide as low a noise figure as could be obtained from a balanced crystal mixer using advanced versions of the 1N78 series of crystals. Now, however, both tunnel-diode amplifiers (TDA's) and semiconductor-diode parametric amplifiers (paramps) have been successfully made for use at the radar frequency. The latter are considerably more sensitive; however, they are also more complex, and therefore costlier, and probably more difficult to maintain at peak operating efficiency than is the simpler TDA.

The TDA, at its present stage of development, has a noise figure of approximately 6.5 db. If it were used singly, and followed by a conventional balanced mixer, the receiver noise figure would rise to about 6.8 db. Since noise figures of just over 8 db can be obtained with conventional mixers, the margin of improvement would not be large enough to justify the use of a TDA. Even with two TDA's cascaded, the improvement would be insufficient. For this reason, attention has been concentrated on the application of a paramp as an RF amplifier in the AN/MPQ-501 receiver.

After soliciting quotations from a number of firms known to be engaged in paramp development work, an amplifier package comprising varactor mount and input and output circulators was purchased from Texas Instruments, Inc., for laboratory examination (see Plate I). The results of tests on this amplifier are reported in Section 1.3.

1.2 Image-Rejection Mixer

To obtain the full sensitivity of which a low-noise RF amplifier is capable, means must be provided for blocking the image-frequency channel, which is normally open in broad-band radar receivers. Failure to block the image-frequency channel allows noise which is generated

within the RF amplifier at the image frequency to be converted to the IF frequency, thus increasing the noise power output of the receiver compared to what it would be if such conversion were prevented.

The image-frequency output of the low-noise RF amplifier can be blocked by using a filter (e.g., a waveguide cavity) between the amplifier and the mixer. Such a filter, which would have to be broad enough (say 10 MHz in bandwidth) to pass the signal information, but selective enough to reject the image frequency (90 MHz away), is quite realizable, but it would have to be made tunable to accommodate the range of magnetron frequencies experienced with this radar, and is therefore ill-suited to the AN/MPQ-501. A newer technique, not requiring any field adjustment, is to use an image-rejection mixer.

Figure 1 is a schematic diagram of an image-rejection mixer. As may be seen, the mixer requires four crystals, two each in a pair of balanced crystal mixers. A hybrid junction power divider in the local-oscillator line introduces a quadrature phase relationship between the local-oscillator excitation of the two balanced mixers. The signal energy is divided equally in a hybrid tee junction, and the two components are applied in phase to the mixers. As shown in Appendix 1, quadrature IF outputs from the two mixers are obtained. Furthermore, the phase sequence of the outputs is opposite for signal- and image-frequency inputs. If the two outputs

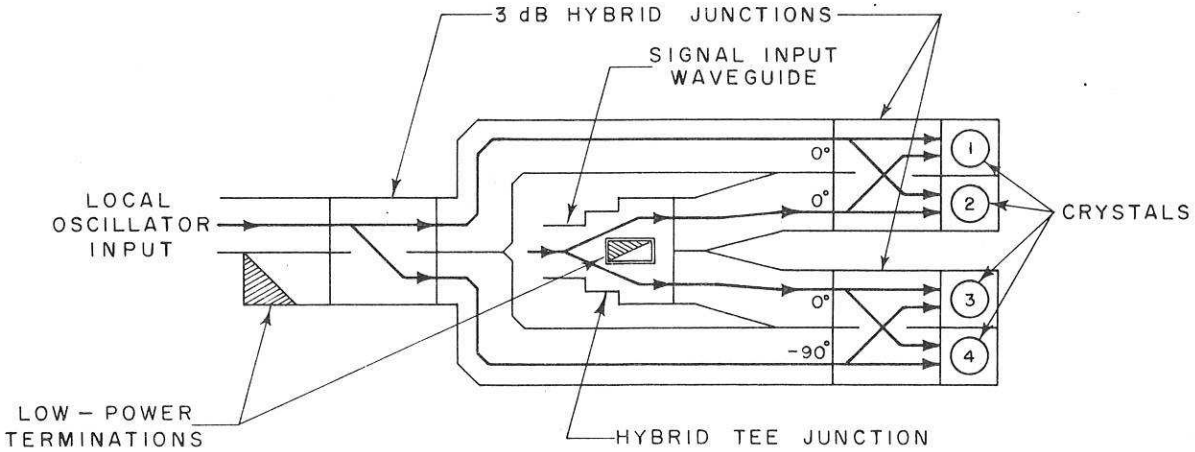

Fig. 1 Schematic diagram of image rejection mixer

are combined using the IF combining network of Fig. 2, IF outputs originating at signal frequency are combined in phase, while outputs which originated at image frequency are combined out of phase, and therefore cancel. Figure 3 shows the circuit which has been built

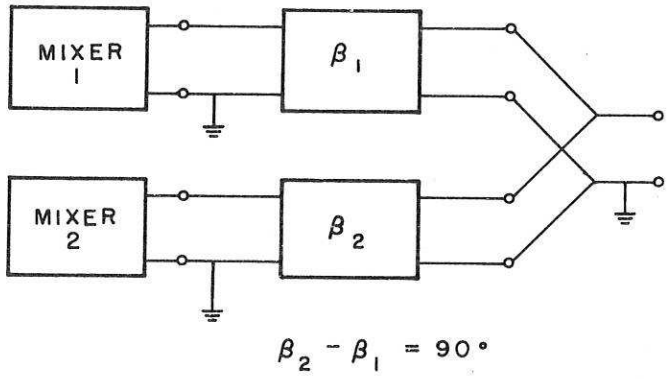

Fig. 2 Block diagram of IF combining circuit

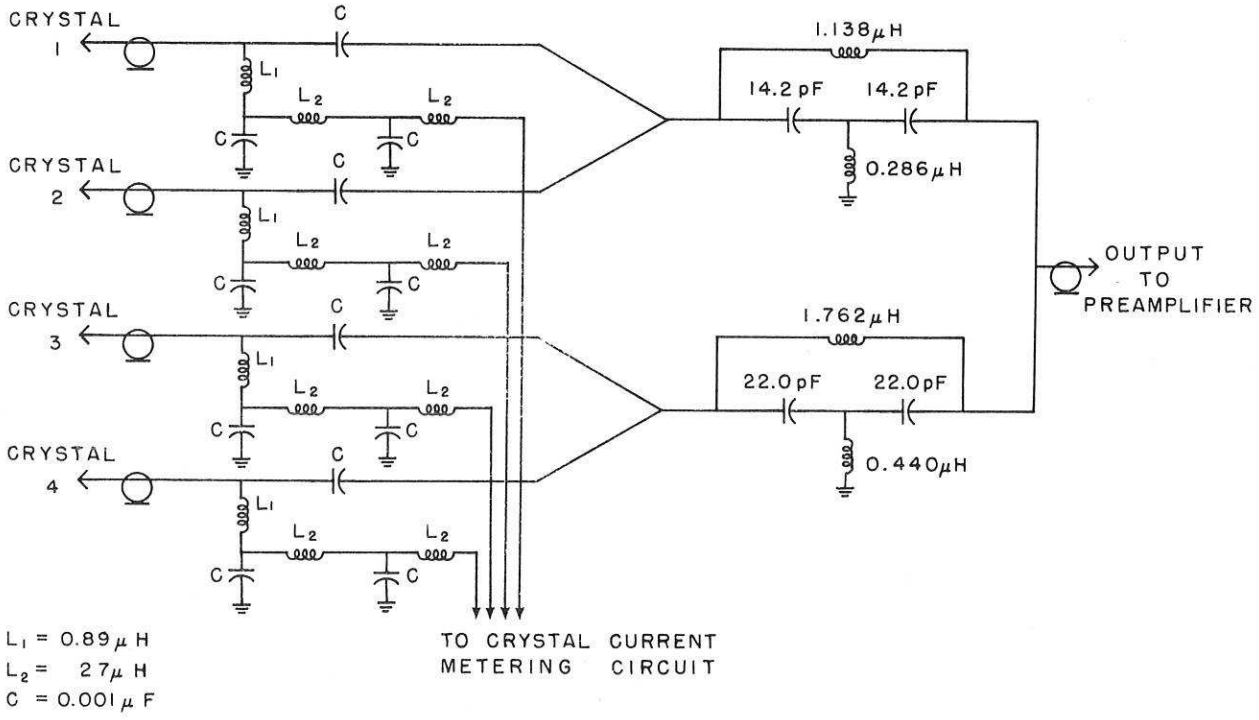

Fig. 3 Schematic diagram of crystal current filters and IF combining circuit

to perform this function. The inductors L_1 are used to resonate the capacitances of the individual crystal holders plus that of the associated cables. The networks comprising inductors L_2 and capacitors C are crystal current filters, and allow for individual metering of the four crystals. The phase-shift networks are of the all-pass variety, and were chosen to provide a phase difference of 90° at 39.1 and 51.9 MHz. The calculated phase difference remains within 90° ± 5° from 36.6 to 55.3 MHz.

The output impedance of such a mixer system is approximately 120 ohms, being the impedance of four crystals in parallel. Since this is just half the value of source impedance for which the IF preamplifier (Unit 29) input network was designed, a revised input network was required. Figure 4 shows the circuit of the preamplifier used with the mixer.

Plate II shows an image rejection mixer assembly made for laboratory use. The four crystal holders are visible at the left. The waveguide at the far right is for insertion of the local-oscillator signal. Of the two remaining waveguides, one is for the signal, while the other is normally terminated. (Either of these two may be used for signal input. Interchanging the connection interchanges signal and image frequencies. For example, if one connection results in cancellation at the sum of local-oscillator and IF frequencies, the other connection will result in cancellation at the difference frequency; i.e., at local-oscillator frequency minus IF frequency.)

The IF combining circuit is shown in Plate III. Considerable reduction in the size of both the image-rejection mixer and the IF circuitry is clearly possible. Since the equipment illustrated was intended for laboratory use only, no particular attempt was made to devise a configuration which would be optimum for incorporation into the existing receiver.

The degree of image reduction is illustrated in Plate IV. This photograph shows the signal (on the left) and image (small double-humped curve) responses of the receiver as a swept signal generator passed through the frequencies accepted by the receiver. The signal-channel band shape is that of the IF amplifier, while the double-humped nature of the image response is a combined effect; the degree of cancellation diminishes near the IF amplifier band edges resulting in a characteristic which rises as the frequency deviates from centre; however, this is soon reversed by the selectivity of the IF amplifier.

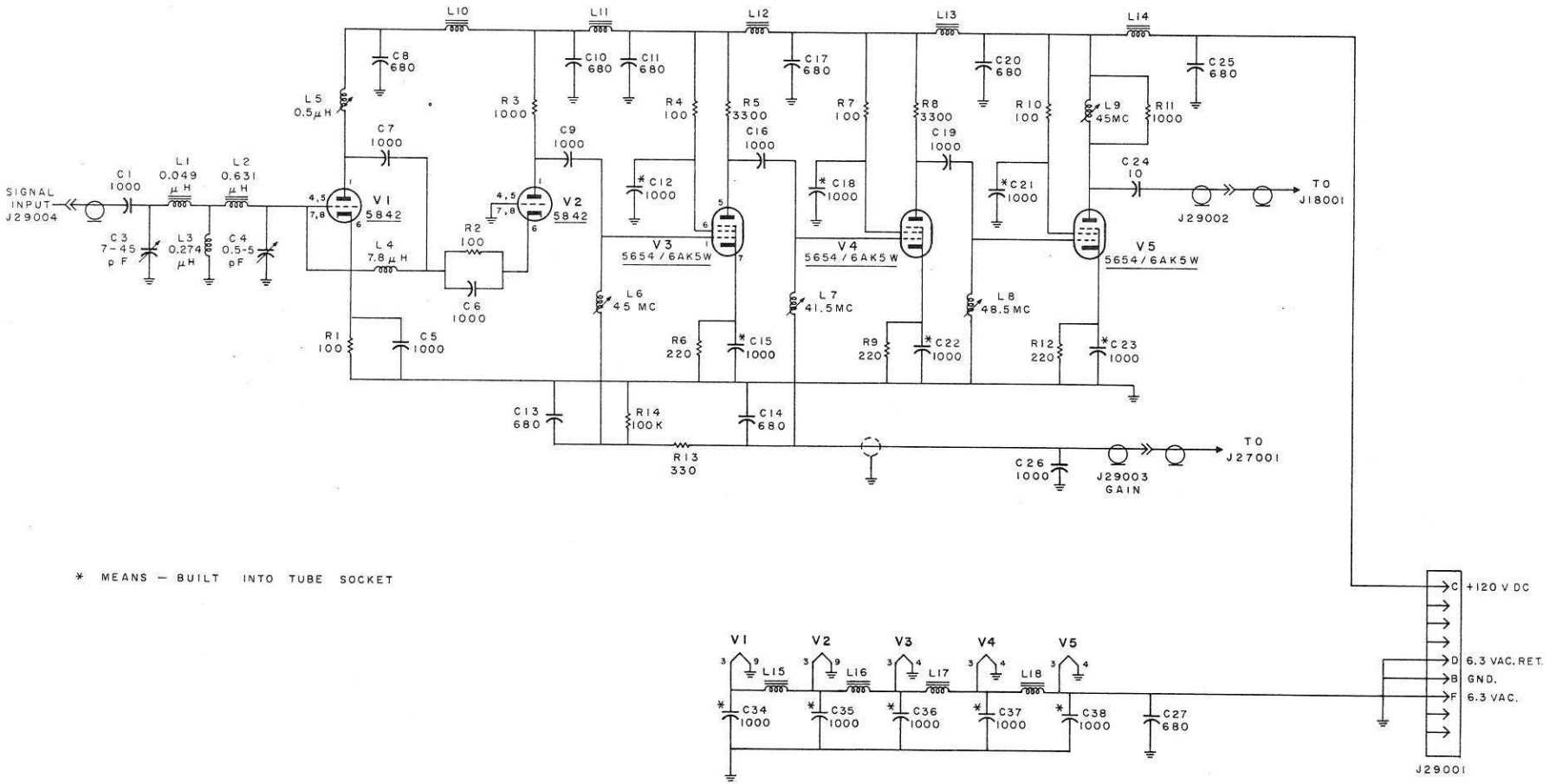

Fig. 4 Revised preamplifier circuit

The cancellation at midband, measured with a calibrated signal generator, was 22.2 db, but this figure deteriorated to 14.8 and 19.2 db at the band edges. By examining the shape of the curve, the effective cancellation over a 10 MHz band was estimated at 16.4 db. It was observed that the shape of the curve changed upon crystal replacement; however, the average value remained approximately the same. With 16.4-db rejection, the image-channel contribution will be less than 0.1 db, assuming that the signal and image channels are equally noisy.

1.3 Parametric Amplifier

The experimental work which has been carried out with the parametric amplifier was designed to determine the amount of sensitivity improvement which could be obtained, and also to obtain first-hand operating experience so that stability (of both gain and frequency), tunability, and adjustability could be assessed. The test set-up used in the laboratory is shown in Fig. 5. The set-up included means for rapidly switching the paramp into or out of the circuit so that gain and noise figure could readily be determined.

The pump klystron selected for use with the paramp was the VA294, manufactured by Varian Associates. Unfortunately, production difficulties with this tube delayed its delivery for a considerable period. Furthermore, the tube, when received, did not provide the 100 mW power output desired. At most, approximately 80 mW could be obtained, using a slide-screw tuned in the pump line. Under these conditions, the maximum gain was 12 db. Subsequently, a VA302D klystron was procured. Although this tube does not cover the entire frequency range recommended by the paramp manufacturer (39.7 ± 0.2 GHz), operation over the lower part of this band with a power output well in excess of 100 mW was possible. With pump power levels of 58 to 78 mW, 15-db gain was obtained within the band 15.7 to 16.3 GHz. This was close to the maximum gain obtainable from the amplifier. Higher pumping levels did not appreciably increase the gain, indicating that the varactor was fully pumped with a pump power of less than 100 mW.

The noise figure of the parametric amplifier has been calculated from measurements of the over-all noise figure of the set-up in Fig. 5. The paramp gain and the second-stage noise figure were also measured. The second-stage noise figure varied between 8.1 db and 8.6 db throughout the tests reported here; various paramp gains varying from 6 to 15 db were used. The paramp noise figure, computed from the usual formula,

$$F_1 = F_{12} - \frac{F_2 - 1}{G_1},$$

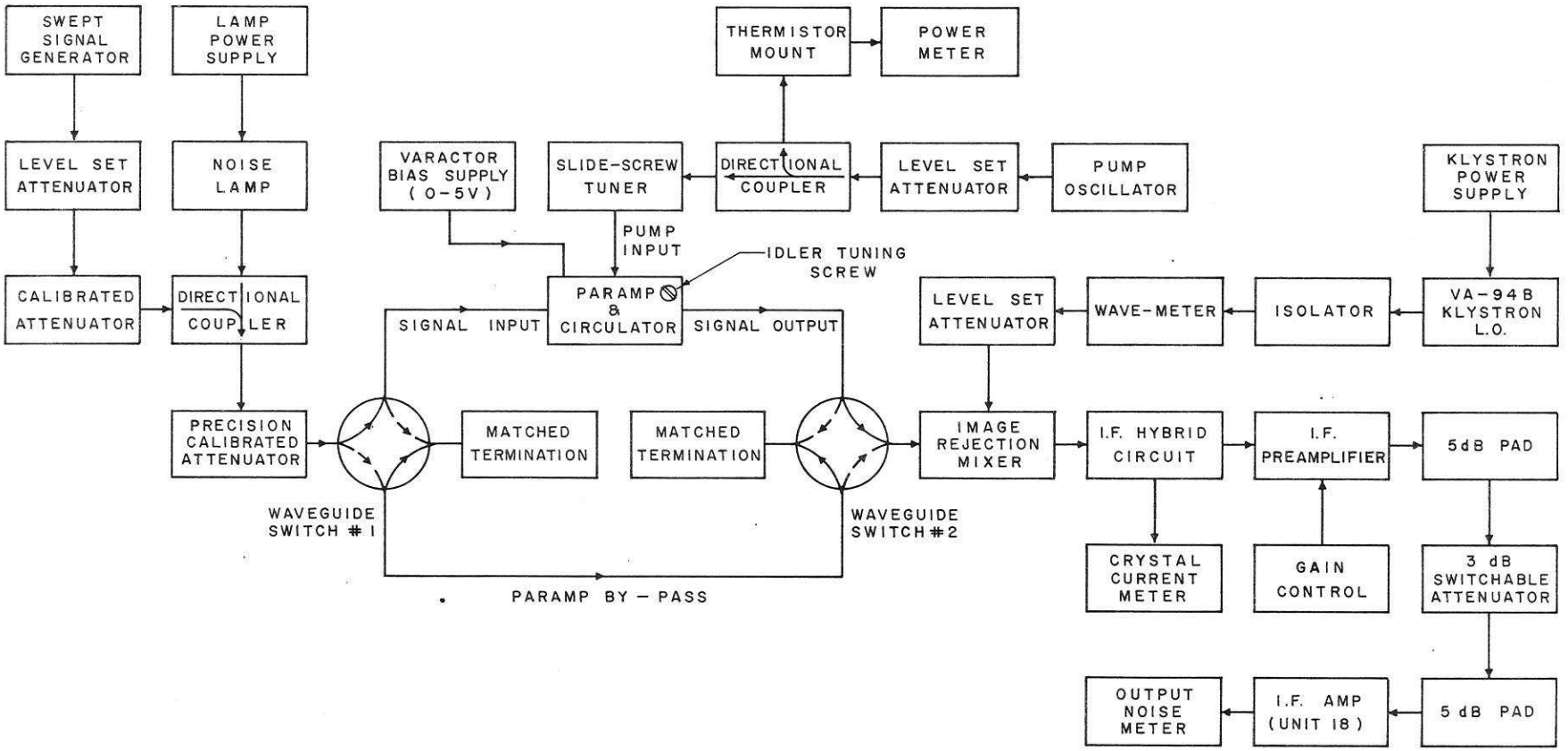

Fig. 5 Parametric-amplifier test set-up

was found to be essentially independent of gain and to have a value of 3.6 db. The over-all noise figure for a paramp gain of 12 db was 4.2 db with a second-stage noise figure of 8.1 db. Assuming that no deterioration in F_1 occurs at the higher pumping level required, an over-all noise figure of 3.9 db would be obtained at 15 db gain. This is an improvement of 4.2 db over the best noise figure that has been obtained with a conventional receiver, and about 5 db over that of the present radar receivers.

All the measurements referred to above were taken with the image-rejection mixer and its matching preamplifier. For purposes of comparison, a conventional mixer and preamplifier were used, and the noise figure was redetermined, all other operating conditions being unchanged. With the image-rejection mixer, an over-all noise figure of 4.3 db (corresponding to a paramp gain of just under 12 db) was observed. When the conventional mixer-preamplifier combination was substituted, the noise figure rose to 5.7_5 db. (Note that this is after allowing 3 db for the image-channel response.) Thus, by excluding noise generated within the parametric amplifier at image frequency, the sensitivity can be increased by approximately 1.4 db.

The voltage gain - bandwidth factor of the paramp was determined at 10-db gain, and was found to be 521 MHz. Thus, since $G^{\frac{1}{2}} B$ is a constant, at 15-db gain the bandwidth should be about 93 MHz, a figure large enough to ensure that the paramp tuning is not critical. The shape of the bandpass appears to be generally that of a single tuned circuit.

All noise figure measurements quoted above are based on the assumption that the noise-lamp output is 16.0 db above room temperature thermal noise. The lamp used was a TD-13/6359 in an RG-91/U waveguide mount, and was operated in the CW mode. It should be noted that many manufacturers use 15.28 db as the reference level, although it is now believed that 16.0 is more accurate (1). (The effect of using the lower figure is to make the equipment appear better than it really is. For example, if the value 15.28 db were used, the paramp noise figure would appear to be 2.9 db.)

Of considerable interest in this application is the ease with which the paramp may be tuned. There are three ways in which the tuning may be accomplished; these are (a) by changing the pump frequency, (b) by tuning the idler cavity, and (c) by varying the bias on the varactor. (The signal cavity is fixed tuned, and is sufficiently

broad-band to permit operation at any frequency at which the MPQ-501 may operate.) In general, it was observed that adjustment of the idler cavity is the best way of tuning, and bias variation the least satisfactory. At high pumping levels, the bias must be adjusted to within a narrow range to avoid excessive varactor current. (Excessive current, either forward or reverse, may be obtained with only slight deviation from the optimum bias when the pumping level is high enough to yield 15-db gain.) In practice, it was found that the varactor bias lead could be left open, with only a slight reduction in gain and no impairment of noise figure compared to operation at optimum bias. (Optimum bias results in a slight forward current of approximately 1 to 3 μamperes.) Likewise, operation with self-bias developed across a large resistor (of the order of 220 kΩ) provides near optimum conditions, while automatically safeguarding against excessive current, which could impair the noise figure and damage the varactor.

For field operation, the pump klystron should be operated at fixed frequency. The following controls will be required:

Pump power level set attenuation
Idler tuning adjustment

These should be remotely controlled from the display area. Tuning of the paramp by observation of permanent echoes (PE's) will probably be satisfactory; however, establishment of the proper gain requires some measurement procedure.

Insufficient gain will not produce the anticipated sensitivity improvement and will therefore be evident from noise-figure measurements. With the particular amplifier tested, excessive gain is not a problem, and satisfactory operation may be obtained by simply maximizing the gain, provided that there is no appreciable degradation in its maximum gain with aging of the equipment. In general, however, it is possible for paramps to become unstable and to oscillate if pumped sufficiently vigorously. Since future versions of the paramp may exhibit such a characteristic, it is desirable to have a means for measuring the gain, and a procedure for setting it to the desired value.

Fortunately, the built-in noise lamp in the AN/MPQ-501 provides such a means without the need for a signal generator. With the noise lamp operating, the increase in receiver noise-power output as a result of application of pump power to the paramp can be used to determine its gain. In practice, it is better to insert attenuation into

the receiver as the pump power is applied so that the same noise output is retained. The amount of attenuation inserted may then be used as a measure of gain. The following expression (derived in Appendix 2) relates the amount of attenuation L to the paramp gain G_1:

$$L = \frac{F_2 + \frac{a}{2}\left(\frac{T_\ell}{T_0} - 1\right)}{G_1\left[F_1 + \frac{F_2 - 1}{G_1} + a\left(\frac{T_\ell}{T_0} - 1\right)\right]}$$

Here F_2 is the second-stage noise figure, i.e., that of the mixer and IF amplifier. $(T_\ell / T_0 - 1)$ has a value of 38.8, and is the excess noise ratio of the noise lamp, and a is the attenuation, if any, between the noise lamp and the paramp. For the MPQ-501, a may be close to 1 db, owing to the numerous components (e.g., waveguide switches, etc.) between the lamp and the receiver. Figure 6 shows the attenuation required, as a function of paramp gain, plotted for three values

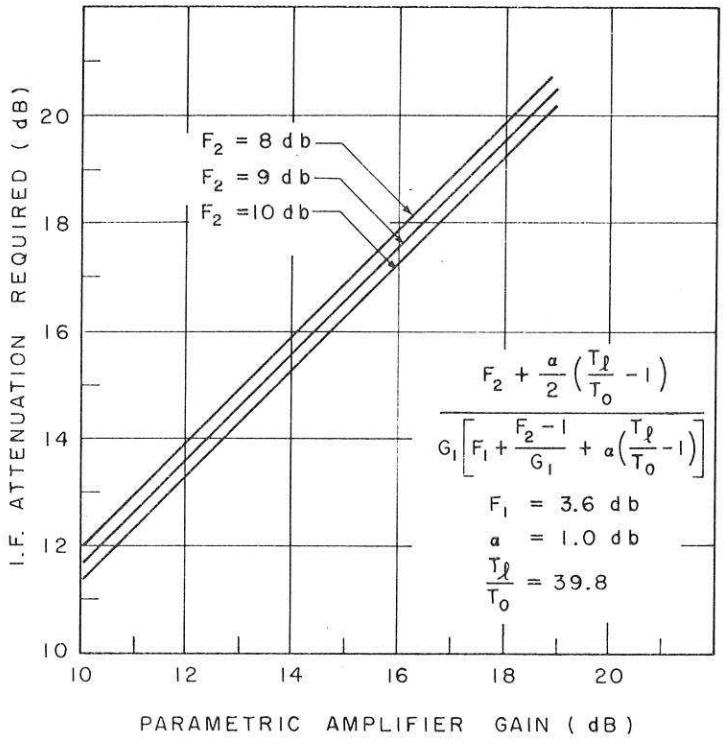

Fig. 6 IF attenuation required for setting paramp gain

of F_2 . A value of 1.0 db was assumed for a. Because a appears as an additive term, the value of L varies more slowly than does a. An uncertainty of ±0.5 db in a is unlikely to be of much concern insofar as its effect on setting the gain is concerned; however, it also enters into the measurement of noise figure, and therefore a should be determined for each radar installation. In the laboratory, this method allows the gain to be set within, at most, 1 db of the desired value.

The following is a practical procedure for setting the paramp gain to a desired value:

1. Tune the receiver to maximize the signals using the manual frequency control, then turn the transmitter off.

2. With pump power fully attenuated, note the receiver noise power output using the meter on the noise monitor. (Without pump power, the paramp behaves as a passive device with about 3-db insertion loss.)

3. Referring to Fig. 6, find the IF attenuation corresponding to the desired value of paramp gain, and insert this attenuation between the IF preamplifier and the main IF amplifier.

4. Increase the pump power in stages, tuning the idler cavity at each stage to maximize the gain, until the original noise power reading is obtained. The paramp gain will now be close to the desired value.

If it is desired to measure the gain of the paramp under a certain set of operating conditions, the following procedure may be used:

1. With the paramp operating, insert IF attenuation in excess of the anticipated gain.

2. Turn on the noise lamp, and note the receiver output power.

3. Remove the pump power.

4. Adjust the IF attenuator until the original receiver noise output is obtained.

5. Use the change in IF attenuation to determine the gain from Fig. 6.

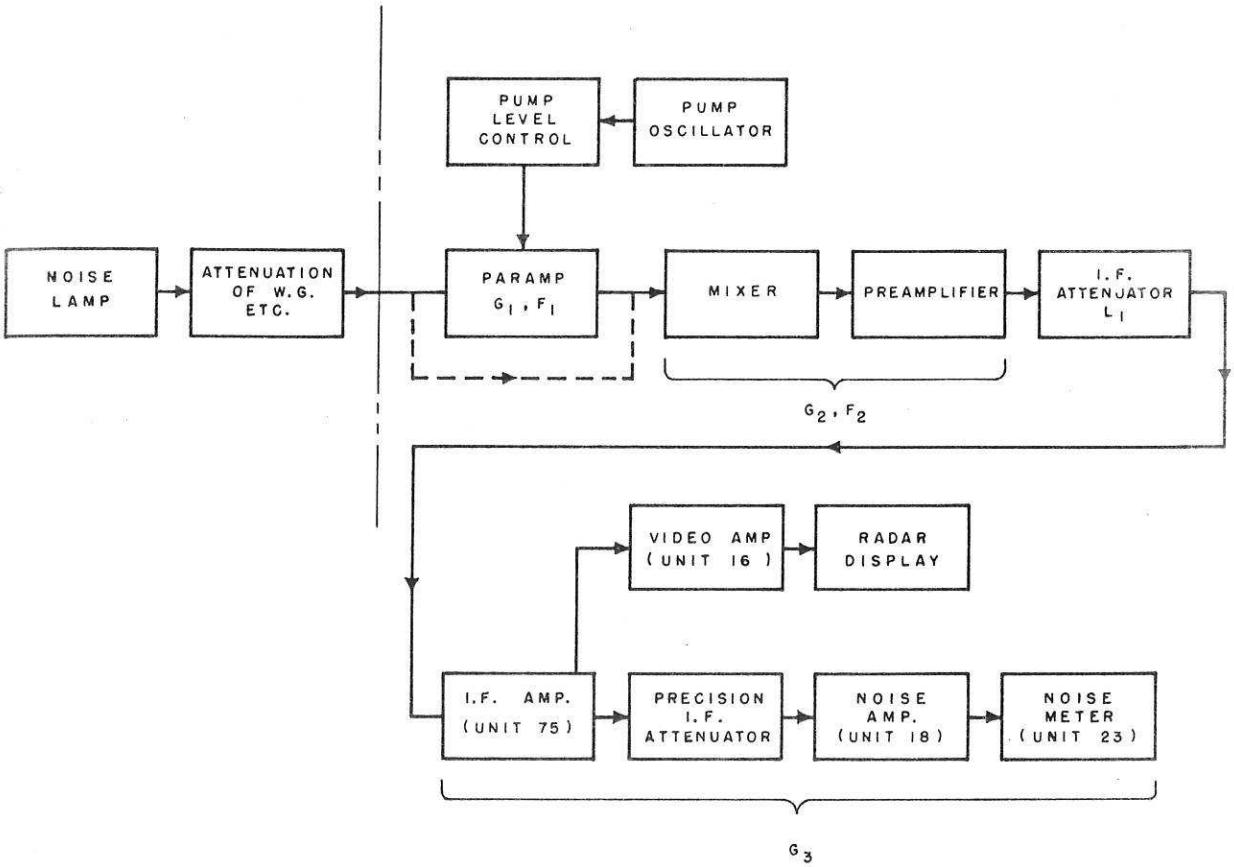

Fig. 7 Block diagram of receiver showing attenuator for setting paramp gain

Figure 7 is a simplified block diagram of the receiver showing the radar noise monitor system and the manner in which it is used to set the gain as described above. The dotted path around the paramp is to be provided by waveguide switches so that the second-stage noise figure may be measured separately. Such a provision would also allow the radar to continue operation with its present sensitivity if the paramp had to be removed for servicing. The IF attenuation should be provided by a new attenuator,

labelled L_1 in Fig. 7. The precision IF attenuator in the noise monitor system is unsuitable, because the dynamic range of the noise channel of Unit 75 will be insufficient for this purpose, even after the modification described in Section 2 below is made.

It is desirable to maintain the same noise level at the video amplifier input, with the paramp operating, as is obtained under the present mode of operation so that the video amplifier is not overloaded. Thus the IF gain must be reduced when the paramp is put into operation. The gain may be reduced either by the pre-amplifier gain control, or by the attenuator L_1 of Fig. 7. Figure 8 shows the required reduction in IF gain for three values of F_2, assuming a paramp noise figure of 3.6 db. (See Appendix 2 for details.)

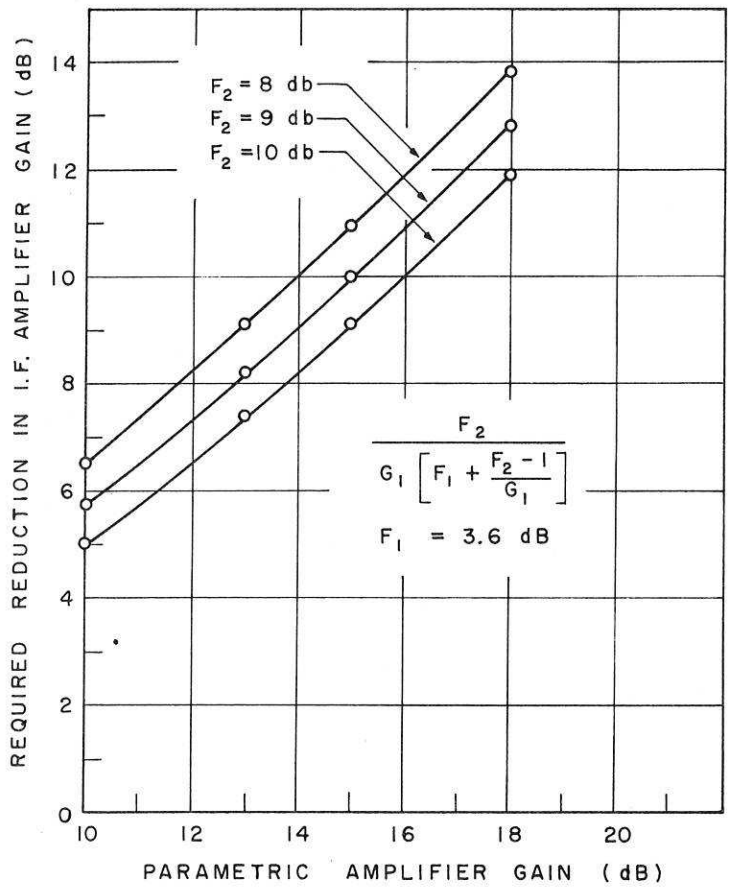

Fig. 8 Required reduction in IF gain to compensate for paramp gain

2. NOISE MONITOR

During the evaluation of a commercial low-noise mixer which had been expected to improve the receiver noise figure by about 2 to 3 db, it was discovered that erroneous noise-figure readings were being obtained with the built-in noise monitor system in radar No. 105. These errors had remained undetected for a considerable period for two reasons: (a) the day-to-day consistency of the readings was good; and (b) the readings, of the order of 12 db, agreed with the manufacturer's results. Widely varying and unrealistic readings, which had been reported earlier on an exported radar, had not been observed on radar No. 105.

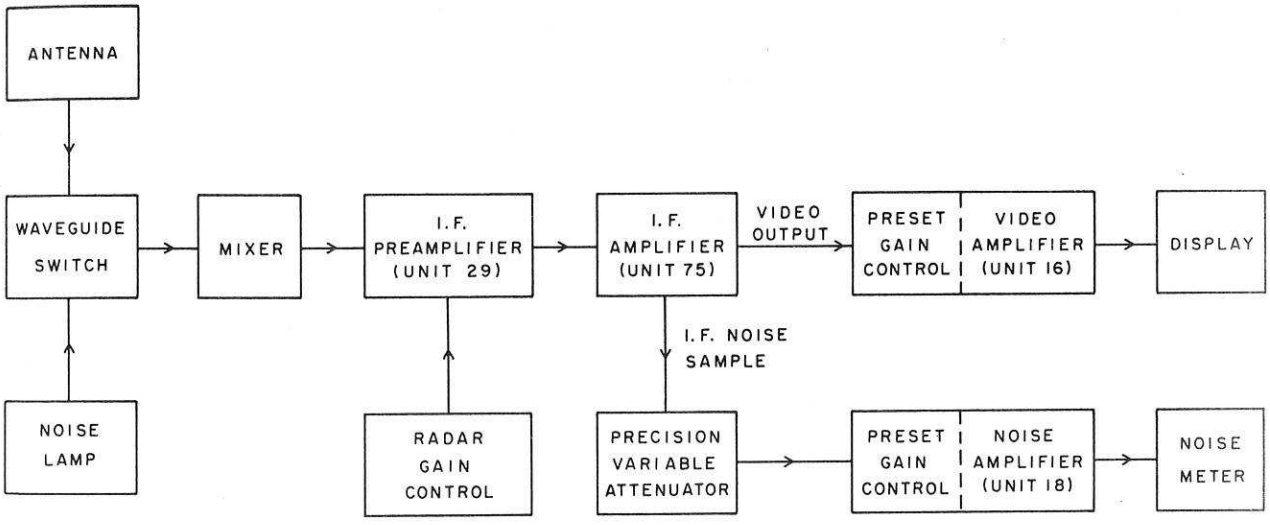

Fig. 9 Simplified block diagram of noise monitor system

Figure 9 shows the noise monitor system in block diagram form. To measure the noise figure, the noise lamp is turned on and connected directly to the receiver input. With typical receiver noise factors, this results in an increase of about 9 to 10 db in the noise power output of the IF preamplifier. For this increase to be reproduced at the noise sample output terminal of Unit 75, the latter must be sufficiently linear that no appreciable compression of the noise takes place. Whether or not such compression does occur depends partly upon the design and partly upon the settings of the various gain controls. As shown in Fig. 9, there are three gain controls involved. These must be carefully

set to obtain proper operation of the receiver and the noise monitor simultaneously. Faulty operation is easy to obtain. For example, if the gain control on the noise amplifier (Unit 18) is fully advanced, it may be necessary, to obtain the specified noise meter reading, to turn down the radar gain control to such an extent that preamplifier noise no longer predominates. Under such conditions, the noise figure will be very poor, but it will probably be accurately measured. Conversely, low gain in Unit 18 will require a high setting of the radar gain control. Now, the noise figure will be good, but if compression occurs in Unit 75, the indicated noise figure will be high. If the video gain is changed, the radar gain control is likely to be adjusted by the operator to maintain the appearance of the display. Thus, without apparent change in the radar performance, the indicated noise figure may change.

With normal gain settings of the radar, the noise level is sufficiently high that compression of the noise peaks takes place. As a result, the increase in the reading of the noise meter is smaller than it would otherwise be, and the monitor will yield a high reading. With a receiver having a 9.5-db noise figure, readings of 10 to 14 db were obtained, depending upon the gain settings of the preamplifier and noise amplifier. By moving the point from which the noise sample is taken from the last stage (V5) of Unit 75 to the second-last stage (V4), the correct reading of 9.5 db was obtained. All receivers of the production radars are now being modified accordingly.

3. HIGH-POWER TRANSMISSION-LINE COMPONENTS

Considerable difficulty has been experienced due to breakdown of the RF transmission line in the AN/MPQ-501 radar. To protect the magnetron output window, a section of waveguide extending from the magnetron to the duplexer is pressurized to approximately 25 psig. This pressurized section is terminated in a waveguide window, beyond which atmospheric pressure prevails. The effect of this arrangement is to reduce the probability of failure of the output window of the magnetron. Instead, the pressurizing window becomes the element which is most likely to be damaged by arcing, since there are no critical sections between the magnetron and the pressurizing window. Breakdown occurring at or beyond the window probably results in a discharge in the window region.

Initially, glass windows of commercial origin were used in the radar. Although operated at or below their rated power level, many of these failed in the manner shown in Plate V. Upon failure, the loss of pressure owing to leakage through the window usually caused transmitter shut-down before magnetron damage occurred. Failure in the manner just described occurred with several types of window from various manufacturers.

As a temporary measure, thin sheets of dielectric material, e.g., teflon and mica, have been used clamped between waveguide flanges to form pressure windows; however, window life was unpredictable and frequently short.

A third type of pressure window used consisted of a plug of teflon (in the shape of an "H") cemented into the waveguide. These windows, although having excellent low-power electrical characteristics suffered from two defects. The tendency of teflon to "cold flow" caused these windows to lose their sealing effectiveness, particularly under conditions where fairly large temperature variations occurred. Secondly, the waveguide system continued to break down after these windows were installed. This resulted in charring and eventual destruction of the teflon plugs. Now, however, because of the construction of the plugs, loss of waveguide pressure did not occur as quickly after arcing started as it did with the glass windows. Consequently, magnetron failures occurred.

Laboratory tests failed to reveal the cause of waveguide breakdown. Subsequently it was learned that the magnetrons used in production radars yielded considerably more power than those available in the laboratory, even although the latter were new. In one direct comparison of both types of magnetron, 50% more power was obtained from the production magnetron than from the laboratory unit. In view of this the occurrence of waveguide breakdown was not surprising.

As one means of protecting the magnetron, a simple system was devised to shut down the magnetron in the event that arcing, or any other fault resulting in a high VSWR, occurred in the radar. This system has been described in a previous report (2) and equipment of this type has now been fitted to production radars.

A second approach to magnetron protection is to pressurize the entire waveguide system, up to and including the slotted radiator in the scanner, thus reducing the possibility of arcing in the duplexer, rotary joint, and antenna. No work has been done on pressurizing

the radiator, although it appears to be feasible. The only other component which presents a serious problem is the rotary joint. Extensive tests (which are being reported separately) on a variety of rotary pressure seals have revealed that dry carbon seals from at least two manufacturers are suitable for this application.

Concurrently, work on a different type of waveguide pressure window has been done. This window, shown in Fig. 10, comprises

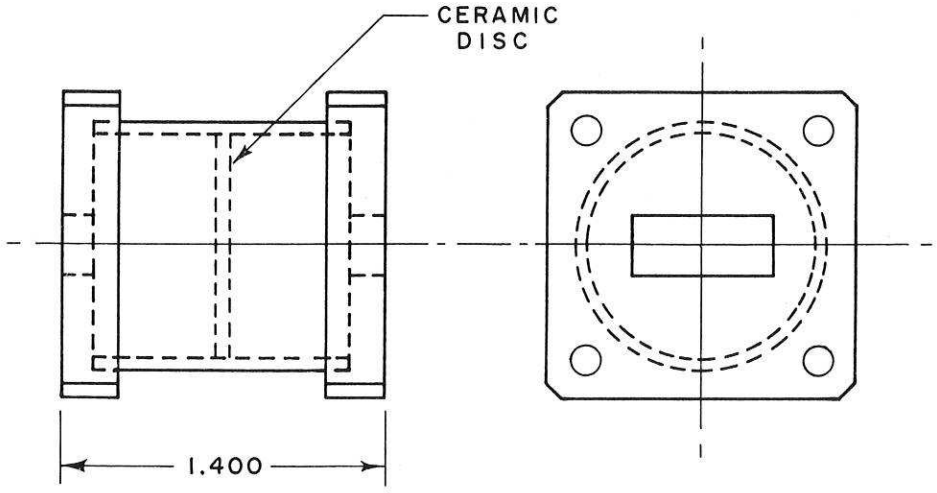

Fig. 10 Ceramic waveguide window assembly

a section of circular waveguide with a thin aluminum oxide disc soldered into the tube in a central location. At each end of the circular tube, abrupt transitions to rectangular waveguide are made (see Plate VI). This design is based on similar devices described by D. B. Churchill (3). The VSWR (see Fig. 11) of two sample windows is less than 1.1 from 15.3 to 16.15 GHz, with the exception of several very narrow peaks which are caused by internal resonances in the ceramic disc. Only one of these lies in the band of interest (15.84 to 16.16 GHz). On three sample windows which have been made, this resonance was undetectable on one, and resulted in VSWR readings of 1.05 and 1.17 on the other two. Although the latter figure is high enough to cause magnetron shut-down with the magnetron protector set for highest sensitivity, it would otherwise be tolerable, considering the narrow frequency region over which it exists. (Fig. 11 exaggerates the width for clarity.) It may therefore be necessary to reduce the protective circuit sensitivity if production versions of this window exhibit this type of reflection.

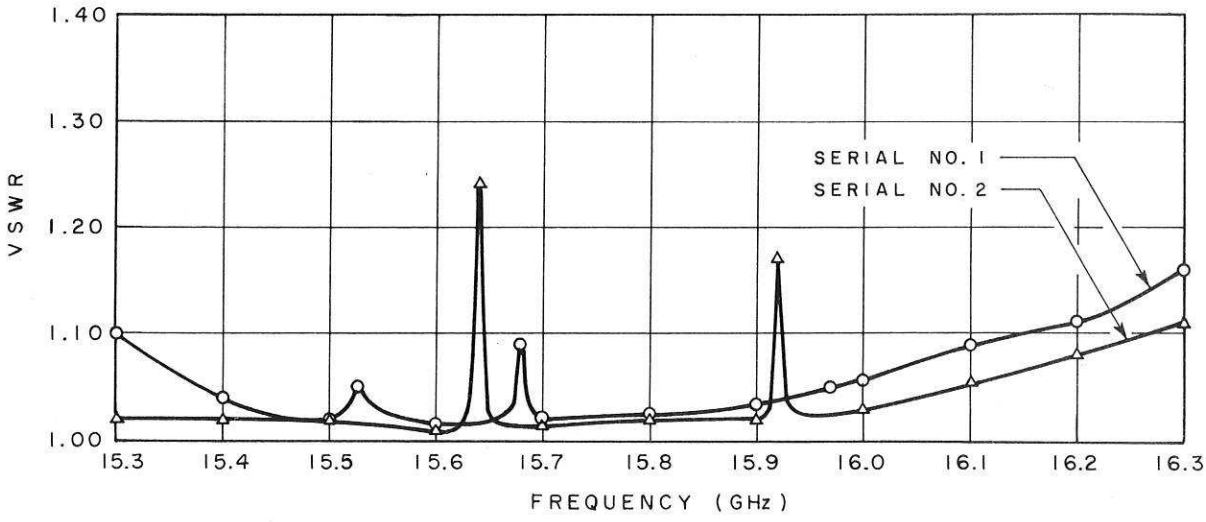

Fig. 11 VSWR of ceramic waveguide windows

The ceramic window described above has been tested in a resonant ring simulator, shown in Plate VII. With such a simulator, components may be subjected to electric field strengths considerably in excess of that corresponding to full magnetron power. Such tests are useful in the determination of breakdown power levels in waveguide components. Figure 12 shows a schematic diagram of the test set-up used for waveguide windows. The window was placed in the test section, and the ring was tuned to resonance by means of the high-power phase shifter. The power level in the ring was monitored by means of a sampling directional coupler and crystal mount, whose output was displayed on an oscilloscope.

Using this system, the ceramic windows operated up to an equivalent power level of approximately 160 kW before breakdown occurred.

4. RADAR PERFORMANCE DEGRADATION DUE TO RAIN CLUTTER

The effects of inclement weather on the detection range obtainable with a short-wavelength radar are severe, principally because of the back-scattered energy from precipitation particles. This energy, which enters the receiver, appears on the display as "rain clutter",

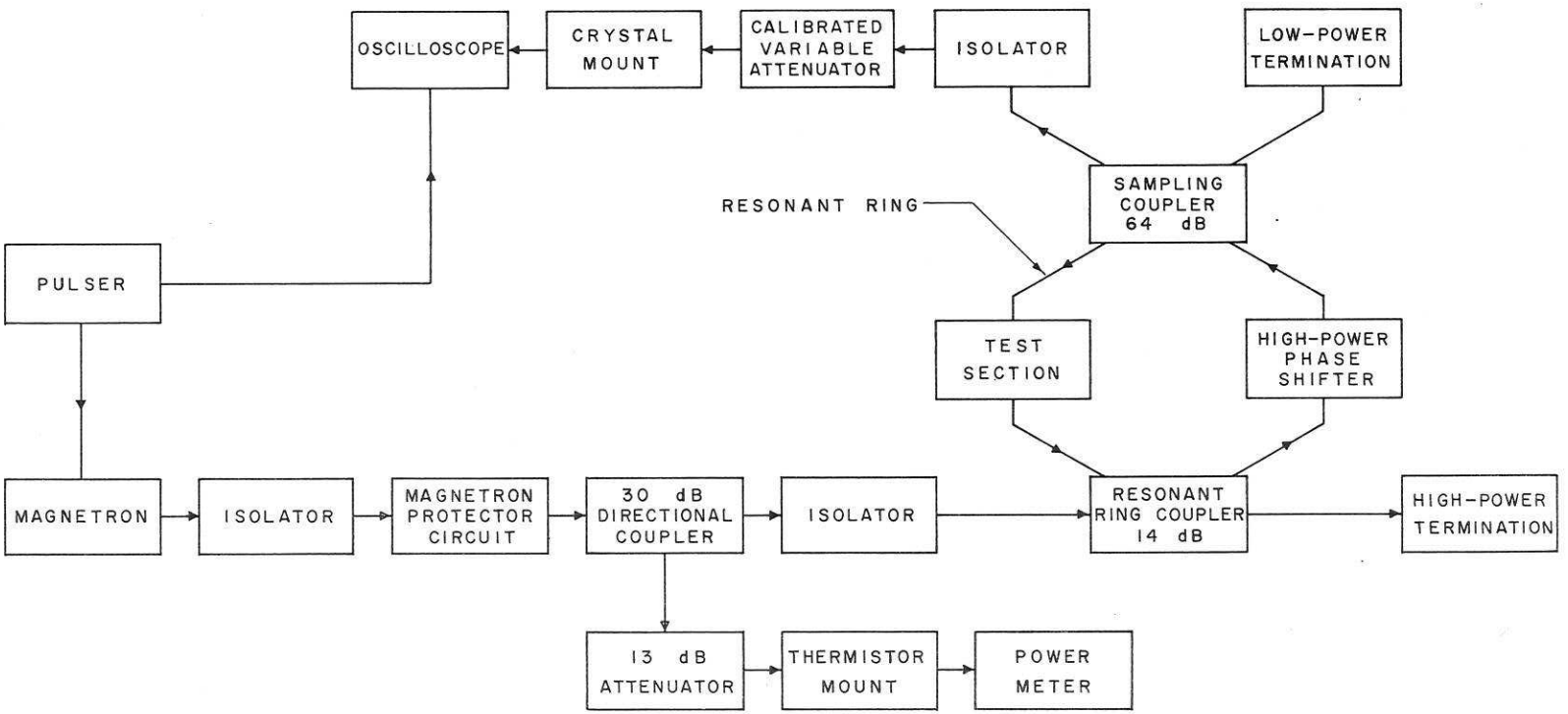

Fig.12 Block diagram of resonant ring simulator

and obscures many targets which would otherwise have been readily detectable. If large enough, this energy may saturate the receiver, thereby preventing the detection of all targets. Although receiver saturation may be made unlikely by the use of wide dynamic-range receivers (such as the logarithmic IF amplifier of the AN/MPQ-501), the near noise-like characteristics of rain clutter make it difficult to remove by video treatment, consequently radar echoes which are weaker than the rain clutter will, in general, be lost.

A second effect, the absorption of energy over the propagation path, is considerably less important in the case of the AN/MPQ-501 radar.

These effects have been summarized in an article by Hawkins and LaPlant (4). By following their method, the performance of the AN/MPQ-501 has been calculated for a variety of weather conditions.

4.1 Atmospheric Effects

The effects of three distinct conditions have been included in the calculations. These are: (a) humidity, (b) fog, and (c) rainfall.

It is assumed, as did Hawkins and LaPlant, that the inclement weather is uniform from the radar to beyond the target, that the entire beam is filled with precipitation, and that the precipitation clutter is uncorrelated. It has been further assumed that the attenuations owing to fog and water vapour are additive.

The various effects are allowed for in the following equation, which is Equation 14 of Hawkins and LaPlant:

$$r_d^4 = r_w^4 e^{kr_w(H\beta+\alpha)} + \frac{r_w^4 P_t A_e c \tau \sigma_u}{8\pi P_n}$$

where r_d is the range, in metres, of the radar against a specific target under dry air conditions; the first term on the right-hand side is the attenuation term, in which

r_w = range (metres) against the same target under inclement weather conditions
α = rainfall attenuation, one way (db/metre)
β = water vapour attenuation factor, one way (db/metre/gram/metre^3)
H = absolute humidity (gram/metre^3)
k = 0.461

The second term of the RHS is the back-scattering term, in which

P_t = transmitted power (watts)

A_e = effective antenna area (metre^2)

c = velocity of propagation (metre/sec)
τ = pulse length (sec)
σ_u = back-scattering cross section per unit volume (metre^2 /metre^3)
P_n = thermal noise power in receiver (watts)

The calculations were made for the following conditions:

Parameter	
T	70°F
H	18.6 gram/metre^3
λ	1.87 cm
G_{ant}	44.4 db
τ	2×10^{-7} second
P_n	4×10^{-3} watts
P_t	7×10^4 watts

Rainfall rates of $\frac{1}{4}$ (drizzle), 1 (light), 4 (moderate), and 16 (heavy) mm/hour, widely used in the literature, have been used. Fog conditions sufficient to limit visibility to 100 feet and 200 feet have been used.

4.2 Circular Polarizer Effects

The polarizer has the following effects:

1. Ohmic and reflection losses are introduced; $\frac{1}{4}$-db loss each way (i.e., transmit and receive) has been allowed for these losses.

2. The returned echo power from a linearly-polarized reflector, oriented co-linearly with the normally radiated polarization, is reduced to $\frac{1}{4}$ (i.e., 6-db loss) of that echo power which would have been received in the absence of the polarizer. (It is interesting to note that if such a reflector had been oriented at right angles to the normally

radiated linear polarization, there would, in theory, have been no return without the polarizer, but with the circular polarizer, a return equal to that obtained above would be seen.)

3. The echo power at the receiver arising from a spherical object in the beam is reduced markedly, compared with the power that it would have returned in the absence of the polarizer; this factor has been taken as 20 db.

4.3 Influence of Circular Polarizer on r_w

For purposes of comparison, r_w with polarizer as a function of r_d without polarizer has been determined. The necessary modification of the basic equation (Equation 14 of Hawkins and LaPlant) may be obtained as follows:

Consider the following cases:

Case 1. Dry air, no polarizer. The signal-to-noise ratio is

$$\frac{S}{N} = \frac{P_d}{P_n} = \frac{P_t G^2 \lambda^2 \sigma_T}{(4\pi)^3 r_d^4 P_n} \qquad (1)$$

where P_d = power received from the target in dry air.

Case 2. Rain, polarizer in use. The signal-to-noise ratio now is

$$\frac{S}{N} = \frac{P'_w}{P_n + P'_c} \qquad (2)$$

where P'_w = power received from the target during rain with the polarizer in use. P'_c = back-scattered power received from rain with the polarizer in use.

Using the radar range equation, one obtains

$$P'_w = L \frac{P_t G^2 \lambda^2 \sigma_T}{(4\pi)^3 r_w^4} \psi \qquad (3)$$

where L is the loss factor (6.5 db) associated with effects 1 and 2 of the polarizer; and $\psi = e^{-k r_w (H\beta + a)}$ is the correction factor to account for attenuation over the path of the beam. Similarly,

$$P_c' = q \frac{P_t G^2 \lambda^2 \sigma_c}{(4\pi)^3 r_w^4} \psi \qquad (4)$$

where q is the fractional reduction of received clutter power owing to the action of the polarizer. σ_c is the effective radar cross section of the rain, i.e.,

$$\sigma_c = \sigma_u V \qquad (5)$$

where V is one-half the volume occupied by a pulse packet (see Ref. 4, p. 27).

Substituting

$$V = \left(\frac{c\tau}{2} \cdot \frac{\pi r_w^2 \theta^2}{4} \right) \qquad (6)$$

where θ = half-power beamwidth of a conical beam, and $\theta^2 = \frac{16}{G}$, the following expression is obtained, assuming the same signal-to-noise ratio for Case 2 as for Case 1:

$$\frac{P_d}{P_n} = \frac{P_w'}{P_n + P_c'}$$

or

$$\frac{P_t G^2 \lambda^2 \sigma_T}{(4\pi)^3 r_d^4 P_n} = \frac{L \frac{P_t G^2 \lambda^2 \sigma_T}{(4\pi)^3 r_w^4} \psi}{P_n + q \frac{P_t G \lambda^2 \cdot 2c\tau\pi\sigma_u}{(4\pi)^3 r_w^2} \psi}$$

whence

$$r_d^4 = \frac{r_w^4}{L\psi} + \frac{q}{L} \frac{r_w^2 P_t G \lambda^2 \cdot 2c\tau\pi\sigma_u}{(4\pi)^3 P_n} \qquad (7)$$

As a check, set L = q = 1, i.e., no polarizer, and substitute $A_e = \frac{G\lambda^2}{4\pi}$, $\psi = e^{-k r_w(H\beta + \alpha)}$; the following equation is obtained:

$$r_d^4 = r_w^4 e^{k r_w(H\beta+\alpha)} + \frac{r_w^2 P_t A_e c \tau \sigma_u}{8\pi P_n}$$

which is Equation 14 of Hawkins and LaPlant. By comparison of the latter with (7) above, it may be seen that the first term of the RHS must be multiplied by $\frac{1}{L}$, and the second term by $\frac{q}{L}$, to take account of the action of the polarizer.

For the polarizer being considered, $L = \frac{1}{4.56}$ (i.e., -6.5 db) $q = \frac{1}{100}$ (i.e., -20 db);(see Section 5 below). Thus, the modified equation is

$$r_d^4 = 4.56\, r_w^4 e^{k r_w (H\beta+\alpha)} + 0.0456 \frac{r_w^2 P_t A_e c \tau \sigma_u}{8\pi P_n} \qquad (7A)$$

Note that 0.0456 corresponds to -13.5 db. Thus, as expected, the loss ratio L applies inversely to the attenuation factor, while the net cancellation of -13.5 db applies to the back-scattered energy.

Figure 13 shows the calculated values of r_w, with and without the circular polarizer. The chart should be entered at the abscissa corresponding to the maximum dry-air range of the radar against a specific target. Moving vertically to the intersection with the curve pertaining to the weather conditions, the inclement-weather range is given by the ordinate of the point of intersection.

An alternative way of viewing the effect of rain clutter is to plot the ratio P_c/P_n vs. range. P_c is the clutter power, while P_n, as before, is the equivalent receiver noise level. This ratio has been calculated for various rainfall rates under two distinct conditions: (a) uniform rainfall throughout the radar beam from target to target, and (b) an isolated rainstorm at the target location, and dry-air conditions elsewhere. The results of these calculations are shown in Fig. 14. As may be seen, the calculated clutter/noise ratio is very large for even the most modest rainfall rates. For case (a), attenuation occurs over the entire path causing the ratio P_c/P_n to decrease sharply at long ranges.

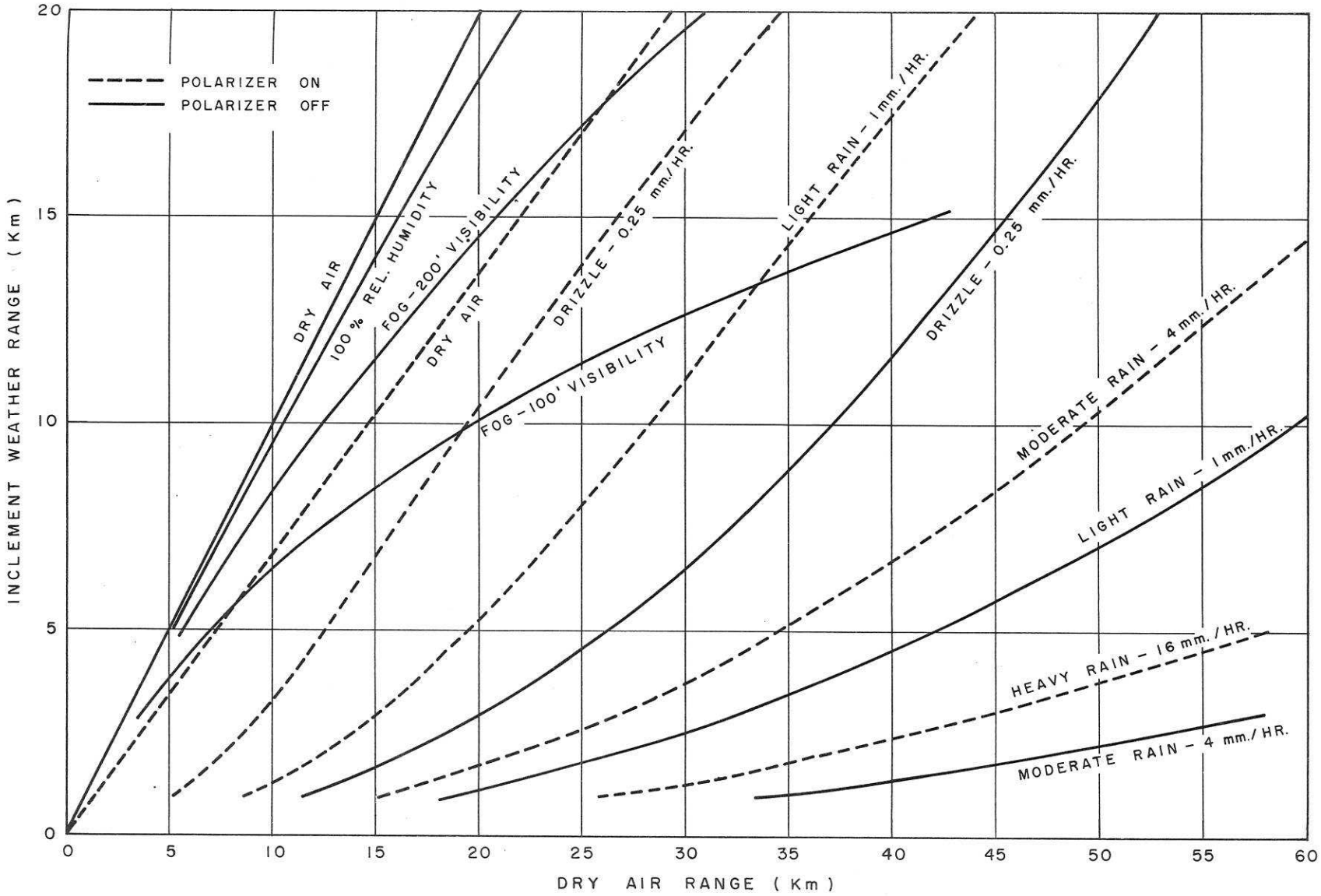

Fig.13 Inclement weather radar range for AN/MPQ-501

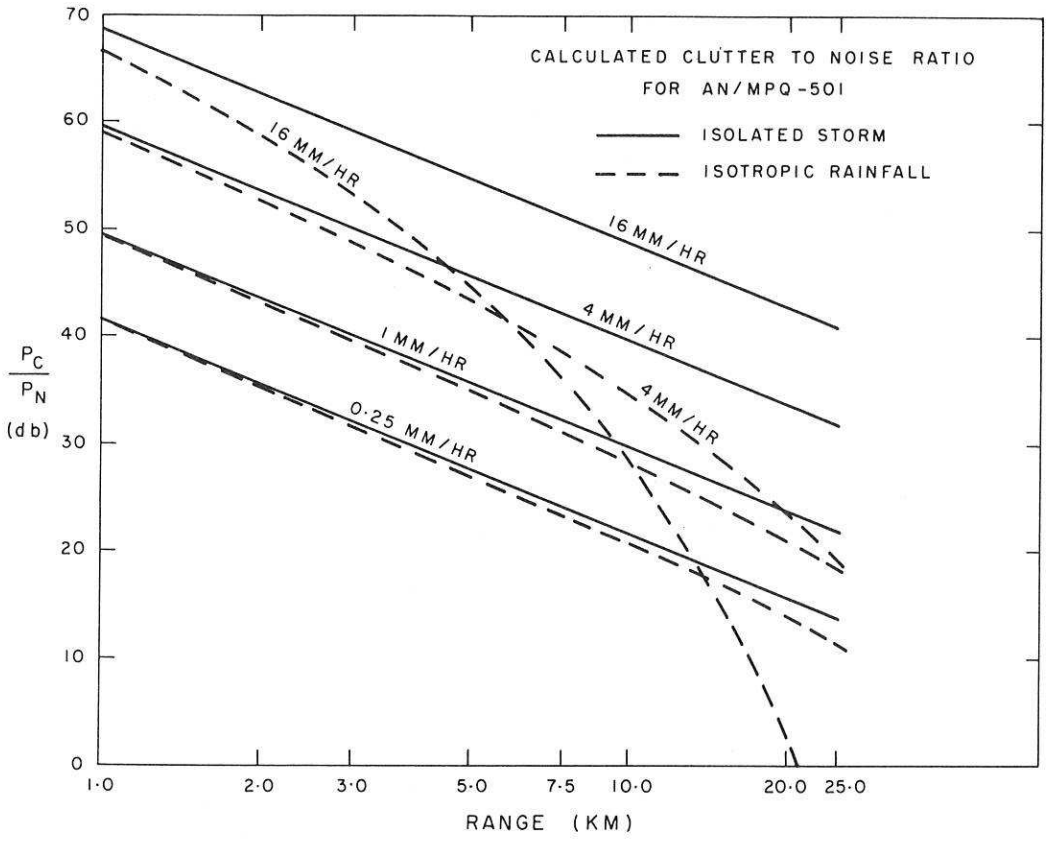

Fig.14 Calculated clutter-to-noise ratio for AN/MPQ-501

By examining the equations quoted above, it may be seen that the back-scattering term may be minimized by using the shortest pulse length and narrowest antenna beam widths which are consistent with achieving the desired dry-air detection range, r_d.

4.4 Experimental Measurement of Rain Clutter

A number of measurements of rain clutter power have been made using the rainfall monitor apparatus described in Appendix 3. The clutter power being returned to the radar from a "cell" some 250 metres long, and subtending an angle of approximately 0.9° at the radar was obtained from recordings of the VCA (voltage controlled attenuator) voltage in the monitor system. (See Fig. 15.)

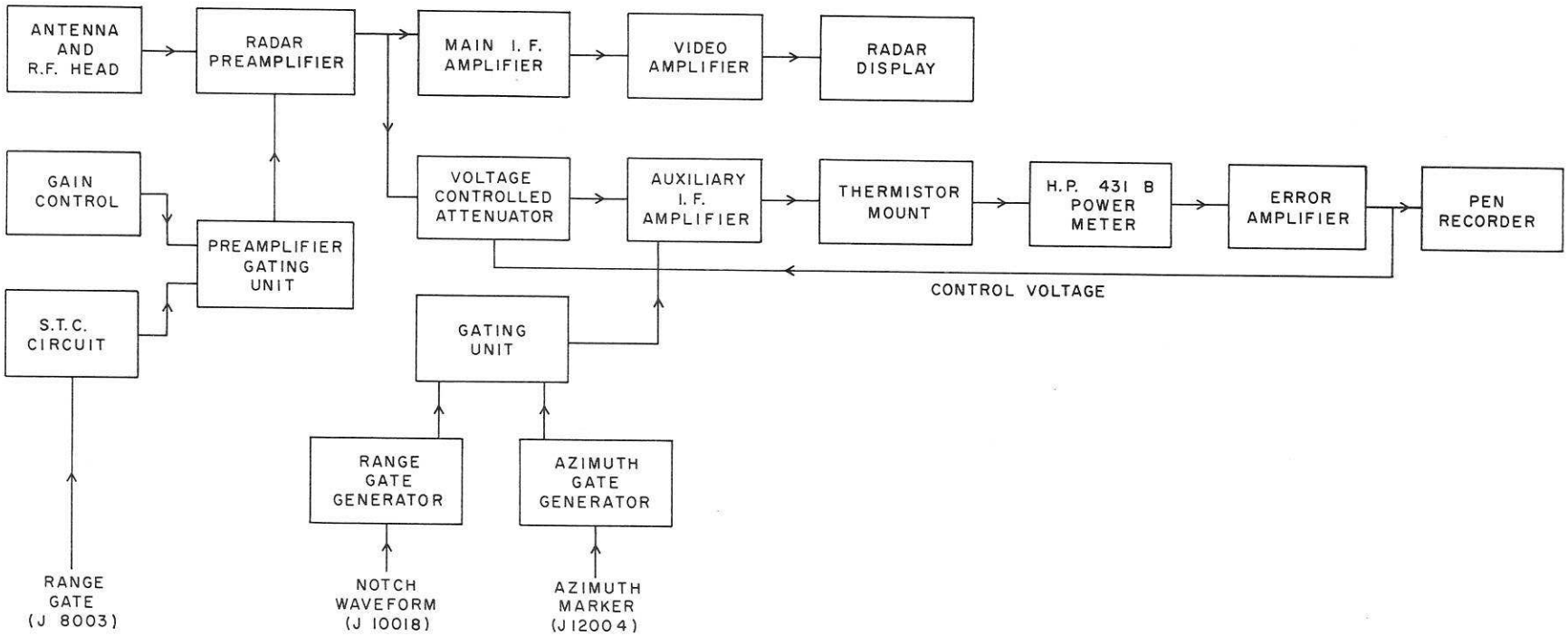

Fig.15 Block diagram of rain-clutter monitor

Simultaneously, recordings of rainfall were made using a tipping-bucket rainfall gauge, which was situated on the ground below the cell being observed by the radar.

Two such rainfall gauges were available for observation from the radar site. These were at distances of 10.1 and 11.1 km respectively. The rain gauges used at these sites provide an indication whenever 1/100-inch of rain has accumulated. From plots of the cumulative rainfall vs. time, the rainfall rate was determined for each rainstorm during which observations were made.

Comparison of the curves of rainfall rate and rain clutter power vs. time indicates rather poor correlation. Frequently, relatively steady clutter 10 to 16 db above receiver noise level was observed with barely measureable rainfall. These echoes have been attributed to clouds from which precipitation was very slight. Excluding such readings, clutter of the order of 12 db below that calculated from the data of Ref. 4 was generally observed. This may have been partly due to absorption over the path; however, as Fig. 14 indicates, at low rainfall rates, the discrepancy is too large to be explained by absorption only. Table I gives the upper bound of clutter-to-noise level observed at various rainfall rates for ranges of 10 to 11 km.

TABLE I

Calculated and Maximum Observed Clutter-to-noise Ratios for AN/MPQ-501 at 10 to 11 km Range

Rainfall rate (mm/hr)	P_c/P_n (Calculated) (db)	P_c/P_n (Observed) (db)
2	34	22
3	35	27.5
4	39	27.5
5	40	26
8	44	30
8	44	32

These results indicate that the curves of Fig. 13 may be unduly pessimistic for rainfall rates of 2 to 8 mm/hour. If the back-scattered

energy is in fact 12 db less than that used in the calculations, the inclement-weather range would be approximately double that indicated. Even so, the effect on radar performance is severe; clutter levels of 22 to 32 db above receiver noise level obscure all but the strongest echoes.

5. POLARIZER MEASUREMENTS

A number of measurements have been made to determine the effectiveness of the circular polarizer against rain clutter. These measurements, which reveal the gross reduction in rain clutter power, measured at the receiver output, were made in three ways. The results, summarized below, show that all three methods are in reasonable agreement.

The first measurements were made with a precision-calibrated waveguide attenuator placed between the duplexer and the receiver-mixer assembly. By switching between linear and circular polarization, the attenuation required to maintain the same degree of clutter on the display under the two conditions of polarization was determined.

Because of the time required to switch between linear and circular polarization (approximately 40 seconds), accurate results are obtainable with this method only if a statistically large number of measurements are made. Individual measurements are subject to error because, in general, storm characteristics change significantly in the switching time, making it difficult to judge the attenuation level required to produce a clutter pattern equivalent to that displayed with the alternate polarization.

The second method of measurement employed a similar waveguide attenuator arrangement; however, for these tests, an artificial echo was injected into the video amplifier from a target simulator. The amplitude of this echo was adjusted so that it was just obscured by rain clutter when circularly polarized radiation was emitted. After switching to linear polarization, the waveguide attenuator was then adjusted to a setting such that the artificial target was again just obscured. The artificial echo could be moved in range and/or azimuth, if necessary, to keep it within the same rain cell. The constancy of the artificial echo is an advantage of this method.

The final method employed to determine the effectiveness of the polarizer used the monitoring system (described more fully in Appendix 3) which automatically sampled and recorded the clutter

power being received from a rain cell approximately 250 metres long by 0.9° wide, lying at a preselected range and azimuth within the lower beam of the radar. The system comprised an auxiliary IF amplifier, sampling and gating circuits, a commercial thermistor mount and power monitor, and a voltage-controlled attenuator (VCA). (See Fig. 15.) The error voltage from the power monitor was used to control the VCA, and thus to maintain a constant output power level from the auxiliary IF amplifier. This error voltage, which was also fed to a chart recorder, was therefore related to the clutter power. For calibration, a CW signal was used, and the error voltage as a function of power level above receiver noise level, was determined. Changes in the recorded output as a result of switching between circular and linear polarization were then used to determine the equivalent change in CW power.

The measurements obtained with these three methods are summarized in Table II.

TABLE II

Summary of Measurements of Polarizer Effectiveness

Measurement method	Region of display	Number of measurements	Average cancellation
1	Centre	19	19.7 db
2	Centre	3	23.5
2	Left edge	3	17.7
2	Right edge	1	22.5
3	Centre	30	19.9
3	Left edge	3	15.5
3	Right edge	4	20.8

No clear evidence of dependence upon rainfall rate was observed. Rainfall rate (when obtainable) varied from less than 0.5 mm/hour to 5.5 mm/hour during the measurements recorded above.

As will be seen from Table II, the centre scan results obtained by Method 3 agree closely with those obtained by Method 1, while Method 2 yields significantly higher readings. This may be due to a change in the character of the clutter when circular polarization is used, such that for a given power at the receiver, the obscuration

of the target is less; however, the total number of measurements with Method 2 is not large enough for such a conclusion to be drawn with complete confidence.

It is of interest to compare these results with cancellation ratios calculated from axial ratios measured on a polarizer of the type used on this radar. McCormick and Barnes (5) report axial ratios of 0.958 to 0.982 for the lower beam of a production polarizer with randomly selected strips. The corresponding cancellation ratios lie between 27.4 and 34.8 db. These figures pertain to the peak of the beam, while the measured values of Table II represent the integrated performance over the entire antenna pattern, including side lobes as well as all parts of the main lobe. Several factors probably contribute to the discrepancy between observed and calculated values of the cancellation ratio. The axial ratios exhibited at the peak of the beam are not likely to be sustained throughout the antenna pattern. Asphericity of the precipitation particles will result in a further imperfection of the cancellation. Multiple scattering, i.e., from droplet to droplet to radar, will likewise reduce the effectiveness of the polarizer.

For comparison, the cancellation provided by the prototype polarizer was measured at centre scan by Method 3. Six readings resulted in an average cancellation of 19.0 db, while seven readings taken with the production polarizer during the same storm averaged 19.7 db.

6. RECOMMENDED AREAS FOR FURTHER STUDY

Several comparatively recent improvements in receiver technology could usefully be incorporated into any future models of the AN/MPQ-501 receiver to improve reliability, and to reduce size, weight, and power consumption.

Broad-band, high-gain IF amplifiers employing transistors instead of vacuum tubes are now widely available. Savings in power consumption would reduce dc power supply sizes.

Ferrite duplexers with associated low-power crystal protector tubes are likely to offer better life than the present dual-TR duplexer, in which the full magnetron power must be switched by the gas tubes.

Solid-state local oscillators are now available for Ku-band, offering improvement in reliability, as well as simplifying the AFC

circuitry and power supplies, since the high voltages required for klystron operation are avoided.

These improvements, in conjunction with the introduction of a parametric amplifier and image-rejection mixer, would update and markedly improve the receiving system.

Because the inclusion of a parametric amplifier would require a major redesign of the RF head, it is recommended that consideration be given to all the items mentioned.

7. ACKNOWLEDGMENT

The author is indebted to Mr. B.D. Stedman, who designed and built the major portion of the clutter monitor system described above, and to Messrs. P.R. Cook, D.T. Bradley, and J.T. Mackey for their assistance.

8. REFERENCES

1. W.E. Wells and J.C. Sadler. Development of Ku-band dual-channel parametric amplifier. Texas Instruments Incorporated. Final Report Contract DA-28-043 AMC-00439 (E) 15 June 1965

2. A. Hendry. An experimental magnetron protector for the AN/MPQ-501 radar. NRC Report ERB-683, September 1964

3. D.B. Churchill. Waveguide windows for high-power microwave tubes. IEEE Convention Record, 7 (III): 154; 1963

4. H.E. Hawkins and O. LaPlant. Radar performance degradation in fog and rain. Trans. IRE on Aeronautical and Navigational Electronics, pp. 26-30; March 1959

5. G.C. McCormick and J.C. Barnes. A polarizer for AN/MPQ-501. NRC Report ERB-636, January 1963

APPENDIX 1

IMAGE-REJECTION MIXER OPERATION

The signal and image paths through a typical image-rejection mixer are shown in Fig. 1. In the analysis below, only relative phases of the various waves are considered; i.e., the phase shifts associated with equal lengths of waveguide are ignored.

Let the local oscillator wave be represented by

$$e_o = E_o \cos \omega_o t,$$

and let the signal be represented by

$$e_s = E_s \cos \omega_s t.$$

If the power division in each hybrid junction (3-db ratio) is taken into account, as well as the 90° relative phase retardation of the coupled signal in a sidewall 3-db hybrid junction, the voltages incident on each of the crystals may be tabulated as follows:

Crystal	Local-oscillator voltage	Signal voltage
1	$\frac{1}{2} E_o \cos(\omega_o t)$	$\frac{1}{2} E_s \cos(\omega_s t - 90°)$
2	$\frac{1}{2} E_o \cos(\omega_o t - 90°)$	$\frac{1}{2} E_s \cos(\omega_s t)$
3	$\frac{1}{2} E_o \cos(\omega_o t - 180°)$	$\frac{1}{2} E_s \cos(\omega_s t)$
4	$\frac{1}{2} E_o \cos(\omega_o t - 90°)$	$\frac{1}{2} E_s \cos(\omega_s t - 90°)$

In addition to these voltages, each crystal is subjected to local-oscillator noise components of random phase. At any given time, however, a given local-oscillator noise component has the same phase relationship to the local-oscillator voltage at all four crystals. Thus, as in the usual balanced mixer, local-oscillator noise cancellation occurs in each of the two balanced mixers.

In the mixing process, which is a result of the nonlinearity of the crystals, the IF output results from a cross-product term. Taking the product of the signal and local-oscillator inputs to each crystal and ignoring all the other terms (which result in dc, fundamental, and harmonic outputs), the significant terms may be written as follows:

Output of crystal No. 1:

$$2K_1 \cos(\omega_o t) \cos(\omega_s t - 90°) = K_1 \Big([\cos(\omega_o + \omega_s)t - 90°] + \cos[(\omega_o - \omega_s)t + 90°] \Big)$$

where K_1 is a conversion-efficiency term and the factor 2 is used for convenience. (Use has been made of the identity $2 \cos x \cos y = \cos(x+y) + \cos(x-y)$.) The second term on the right-hand side of the above expression is the IF term. Similarly, the IF outputs of the other three crystals may be obtained. These four IF voltages are:

$$e_1 = K_1 \cos[(\omega_o - \omega_s)t + 90°]$$

$$e_2 = K_2 \cos[(\omega_o - \omega_s)t - 90°]$$

$$e_3 = K_3 \cos[(\omega_o - \omega_s)t - 180°]$$

$$e_4 = K_4 \cos[(\omega_o - \omega_s)t] ,$$

where K_i is a measure of the conversion efficiency of the i-th crystal.

Note that outputs 1 and 2 are of opposite phase as are outputs 3 and 4. If crystals 2 and 3 are of reversed polarity (i.e., "R" type) then outputs 1 and 2 will be in phase, as will 3 and 4. If, furthermore, the simplifying assumption that $K_1 = K_2 = K_3 = K_4$ (reasonable for matched crystals) is made, then the IF outputs may be written

$$e_1 = e_{2R} = K \cos[(\omega_o - \omega_s)t + 90°]$$

$$e_{3R} = e_4 = K \cos[(\omega_o - \omega_s)t].$$

Note that the two crystal pairs may now have their IF terminals paralleled to produce two IF voltages of equal magnitude and quadrature phase. Furthermore, if $\omega_o < \omega_s$, the phase sequence of these two voltages is opposite to that which prevails for $\omega_o > \omega_s$, since $\cos(-x) = \cos x$. Designating the "image" frequency case by the subscript i, the expressions become:

$$e_{1i} = K \cos[(\omega_s - \omega_o)t - 90°]$$

$$e_{4i} = K \cos[(\omega_s - \omega_o)t] .$$

Cancellation of the image response may be accomplished by the use of the combining circuit shown in Fig. 2, at the output of which signal voltages are in phase, while image voltages are anti-phase and therefore cancel.

APPENDIX 2

METHOD OF SETTING PARAMETRIC AMPLIFIER GAIN USING BUILT-IN NOISE LAMP

The noise lamp may be used to set the paramp gain to a predetermined level by the following procedure. (It is assumed that an image-rejection mixer or other image filter is used.) The method assumes that the "cold" insertion loss of the paramp is 3 db. (This value is in good agreement with the measured value.) The relevant parts of the system are illustrated in Fig. 16.

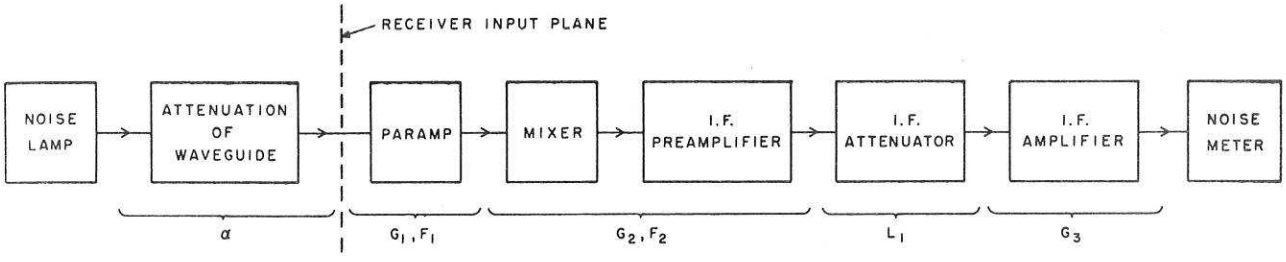

Fig. 16 Simplified block diagram of receiver

With the pump klystron turned off, the paramp is passive, and

$$G_1 = \frac{1}{F_1} \left(= \frac{1}{2}\right)$$

In general, the noise power output of the receiver is:

$$N = G\,FkT_0B \qquad (A1)$$

where $G = G_1G_2G_3$, and $F = F_1 + \frac{F_2 - 1}{G_1} + \ldots\ldots$, provided that the effective source temperature is at $T_0 = 290\,^\circ K$. Equation A1 may be written:

$$N = G[(F - 1)kT_0B + kT_0B] \qquad (A2)$$

in which the first term is amplifier noise, and the second, source noise. If now the noise lamp is fired, the effective source temperature becomes

$$\alpha\left(\frac{T_\ell}{T_0} - 1\right)T_0$$

where T_ℓ is the effective temperature of the lamp and a is the attenuation of the waveguide between the lamp and receiver. (The effective temperature of the elements comprising a is assumed to be T_0.) Thus, with the lamp on, the noise output becomes

$$N_1 = G_1 G_2 G_3 \left[F_1 + \frac{F_2 - 1}{G_1} + a\left(\frac{T_\ell}{T_0} - 1\right)\right] kT_0 B \qquad (A3)$$

which follows from (A2) upon substitution for the source temperature. From A3, if the paramp is unpumped, (i.e., $G_1 = \frac{1}{2}$, $F_1 = 2$), the noise output is:

$$N_1' = \tfrac{1}{2} G_2 G_3 \left[2 + 2(F_2 - 1) + a\left(\frac{T_\ell}{T_0} - 1\right)\right] kT_0 B \qquad (A4)$$

Now, if the paramp is pumped so as to provide gain G_1, and simultaneously, attenuation L_1 is introduced into the IF amplifier chain to maintain noise output N_1', then the following equality holds:

$$L_1 G_1 G_2 G_3 \left[F_1 + \frac{F_2 - 1}{G_1} + a\left(\frac{T_\ell}{T_0} - 1\right)\right] = \tfrac{1}{2} G_2 G_3 \left[2 + 2(F_2 - 1) + a\left(\frac{T_\ell}{T_0} - 1\right)\right]$$

or

$$G_1 = \frac{F_2 + \frac{a}{2}\left(\frac{T_\ell}{T_0} - 1\right)}{L_1 \left[F_1 + \frac{F_2 - 1}{G_1} + a\left(\frac{T_\ell}{T_0} - 1\right)\right]} . \qquad (A5)$$

Equation A5 allows the determination of G_1 from the value of L_1, provided that a, F_1, and F_2 are known. This expression is plotted in Fig. 6 for three values of F_2.

In a similar manner, the reduction if IF gain required to maintain constant noise output when the paramp is switched into the circuit may readily be obtained as follows.

With the paramp out of the circuit, receiver noise output is:

$$N_2 = G_2 G_3 F_2 kT_0 B \qquad (A6)$$

Now let the paramp be switched into the circuit, and IF attenuation of L_1' be introduced. The noise output will now be

$$N_2' = L_1' G_1 G_2 G_3 \left[F_1 + \frac{F_2 - 1}{G_1} \right] kT_0 B \qquad (A7)$$

Equating N_2 and N_2' ,

$$L_1' = \frac{F_2}{G_1 \left[F_1 + \frac{F_2 - 1}{G_1} \right]} \qquad (A8)$$

This expression has been plotted in Fig. 8.

APPENDIX 3

RAIN CLUTTER MONITOR SYSTEM

In order to monitor the received clutter power during rainstorms, the apparatus shown in Fig. 15 was assembled using an AN/MPQ-501 which was temporarily installed in a laboratory building. The top row of blocks in the figure are elements of the radar, while the remainder comprise the monitor system.

An IF output was taken from the radar preamplifier and fed to a voltage-controlled attenuator (VCA). This device, whose insertion loss may be varied from 0 to approximately 60 db, depending upon the magnitude of the control voltage, formed part of a feedback loop containing auxiliary IF amplifiers, a thermistor mount, power meter, and error-voltage amplifier. The power meter used, a Hewlett-Packard type 431B, provides, through an output jack an error voltage proportional to the power fed into it. This voltage was amplified, and fed back to the VCA, thus stabilizing the loop for a given amount of IF power fed into the VCA. A change in the level of IF power due, for example, to a change in the rain clutter, results in a change in the control voltage as the loop seeks to stabilize its gain at the new power input level.

In operation, the control voltage was recorded on a paper chart. The system was calibrated using a signal generator to provide known inputs, and a chart of control voltage vs. input power was plotted for subsequent analysis of the pen-recorder records.

To prevent the transmitter pulse and close-in ground echoes from saturating the system, the radar preamplifier was gated off by a sensitivity - time control (STC) circuit during the initial part of each radar sweep. The STC waveform was added to the normal radar gain control voltage, and applied to the preamplifier as shown.

To examine relatively small rain cells, the auxiliary IF amplifier was gated both in range and azimuth. The azimuth gate waveform allowed information through the IF amplifier on eight successive range sweeps, corresponding approximately to one antenna beamwidth, while the range gate duration was 1.7 μsec, approximately 250 metres in range.

The dynamic range of the system was in excess of 50 db.

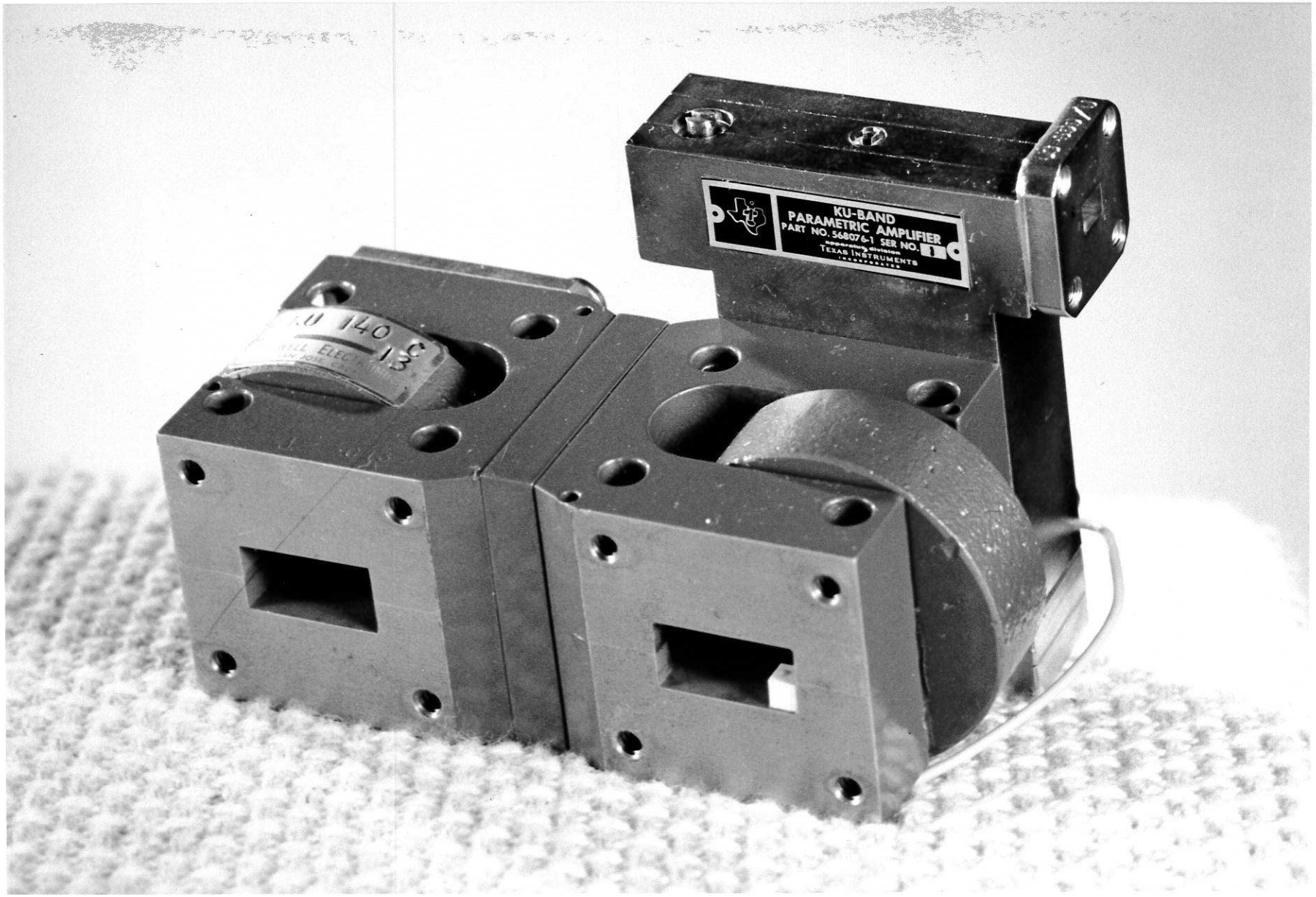

Plate I — Ku-band parametric amplifier

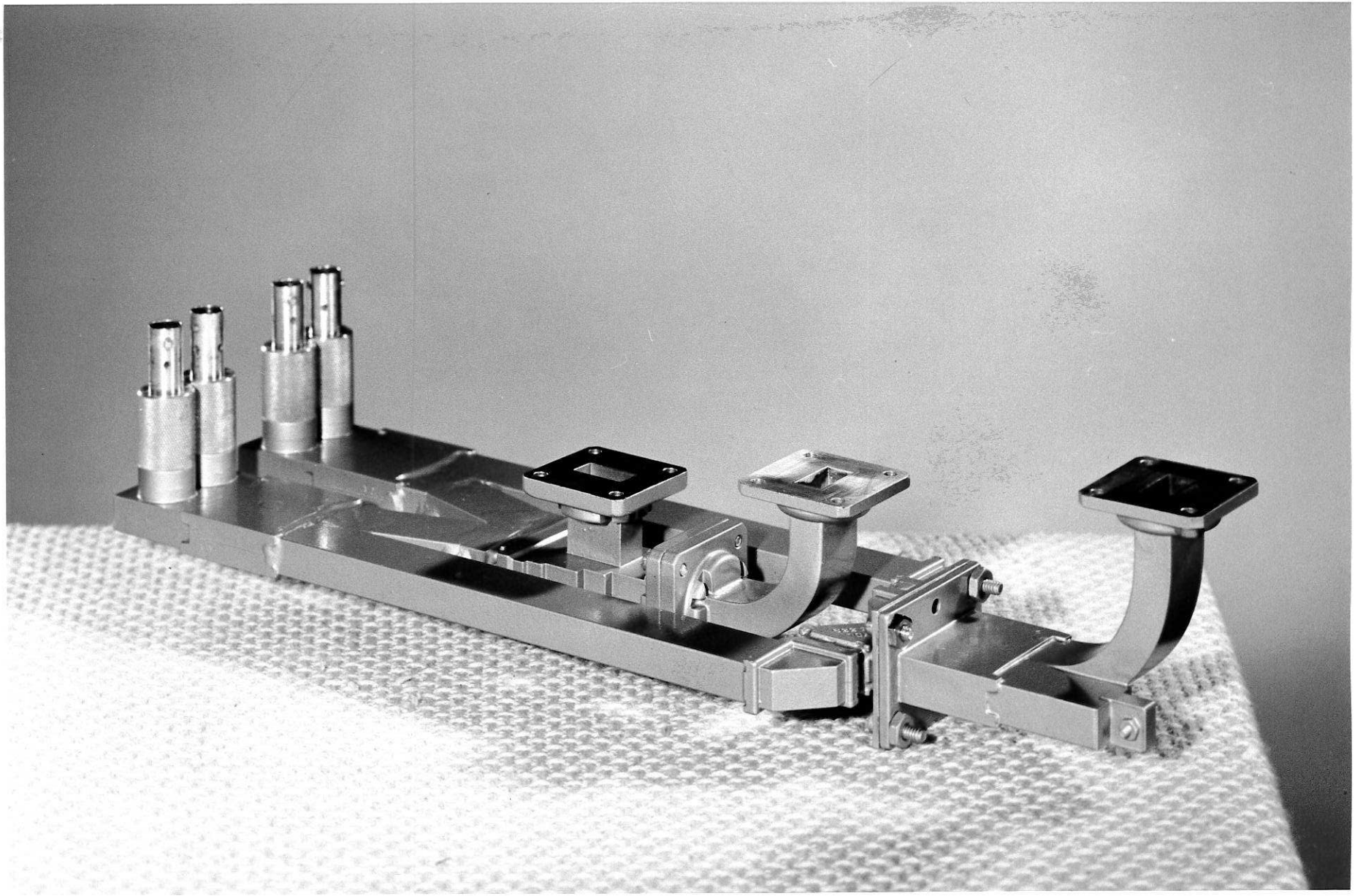

Plate II — Laboratory model of image-rejection mixer

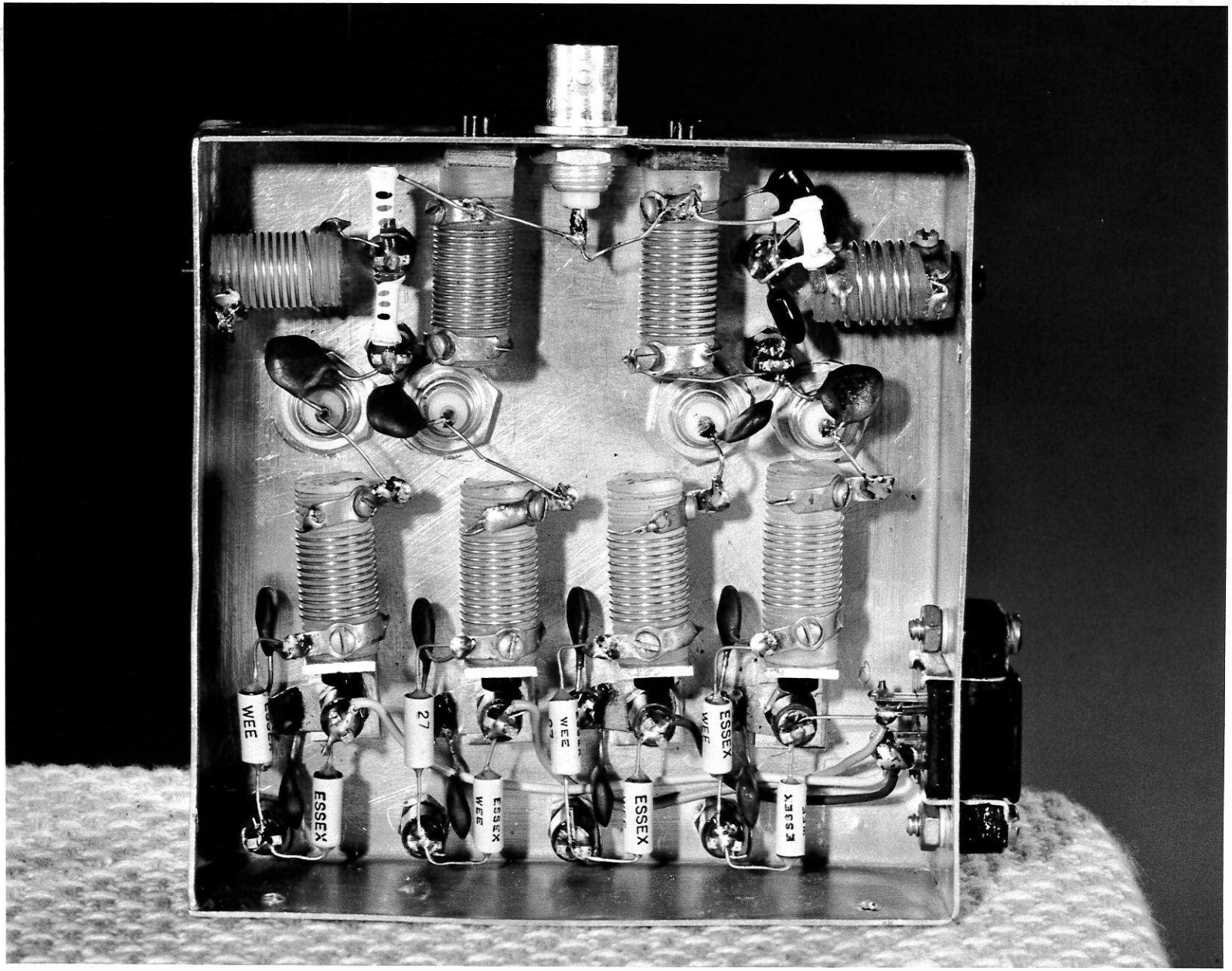

Plate III — Interior view of IF combining circuit

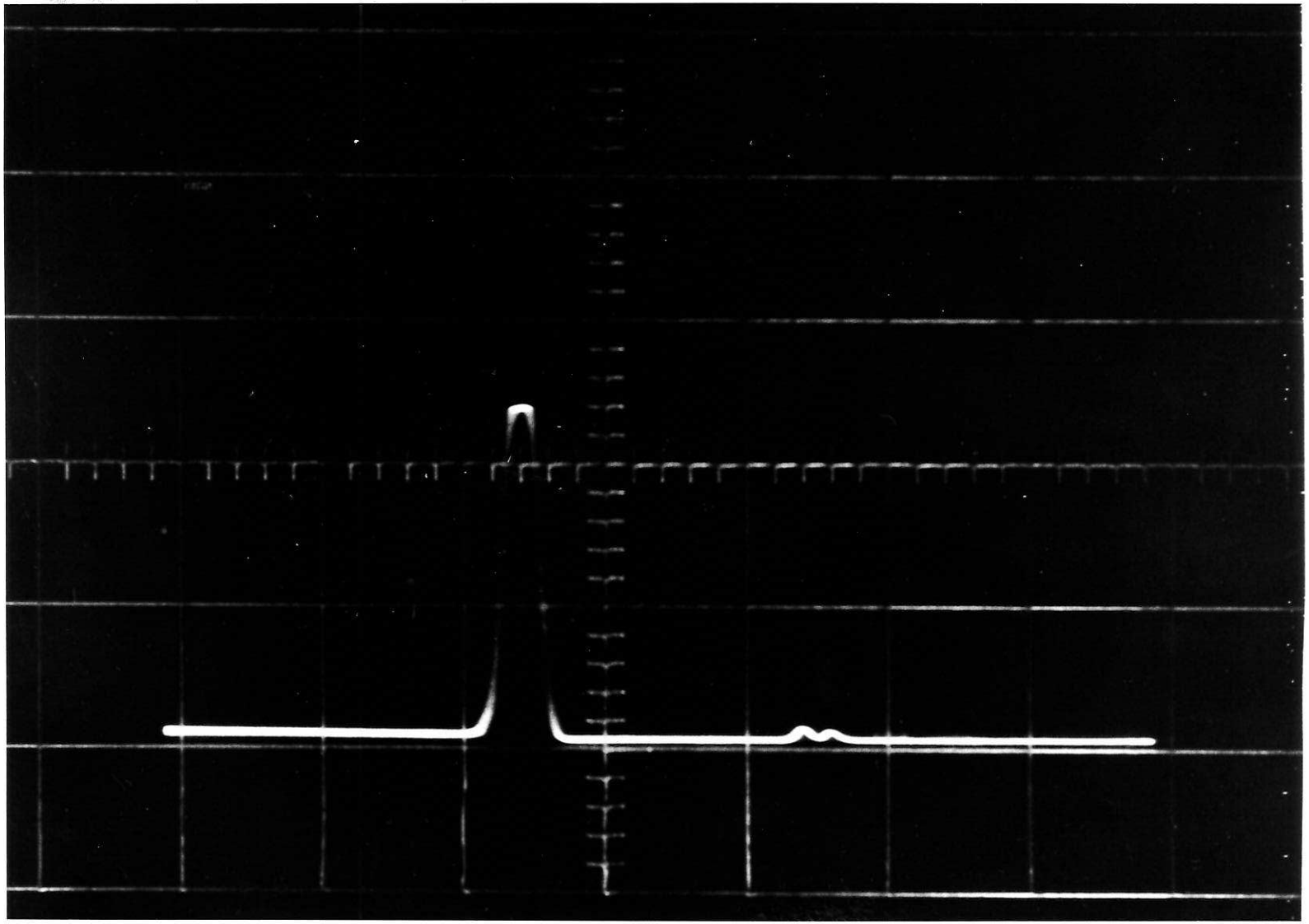

Plate IV — Signal and image response curves of receiver

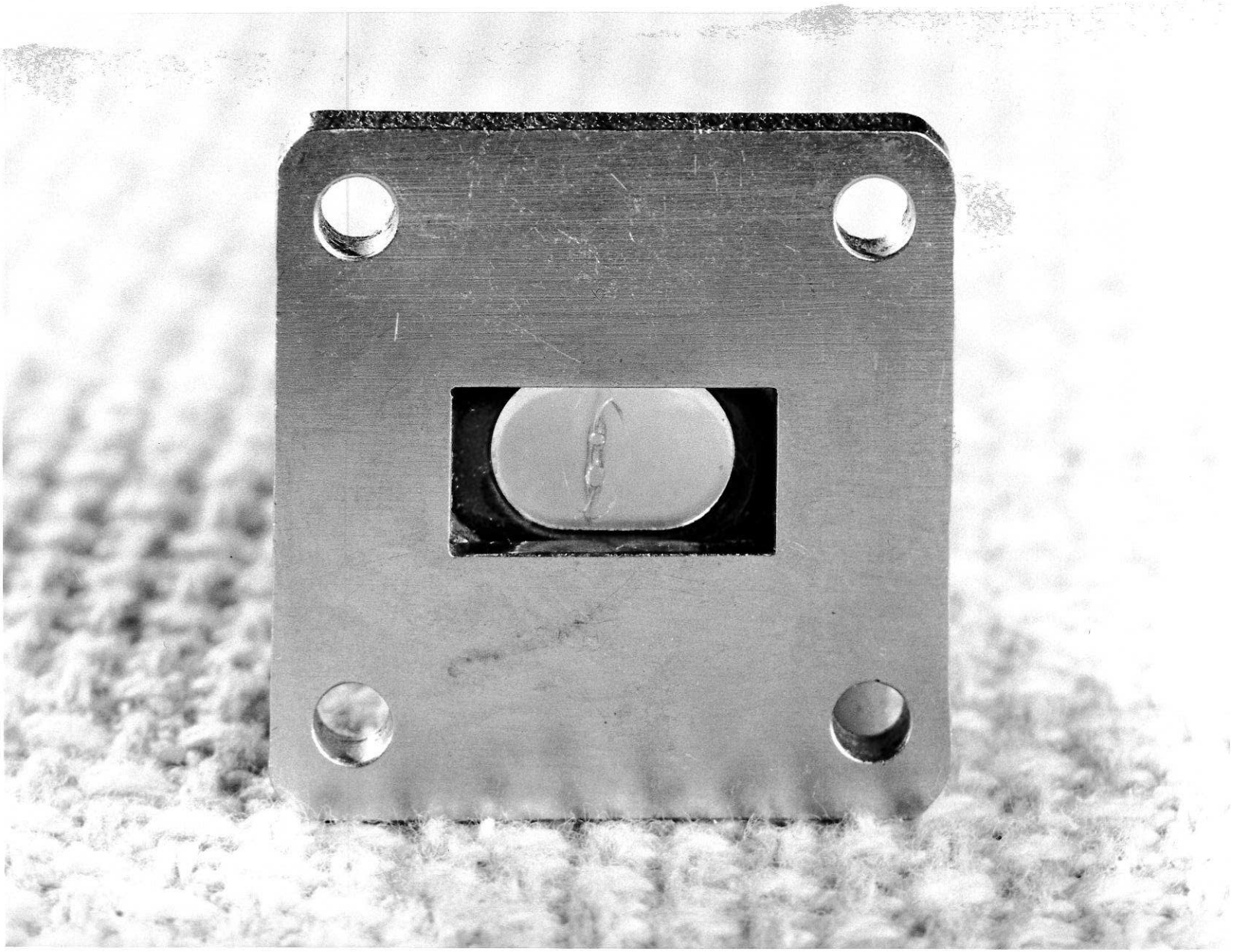

Plate V — Typical failure of glass waveguide window

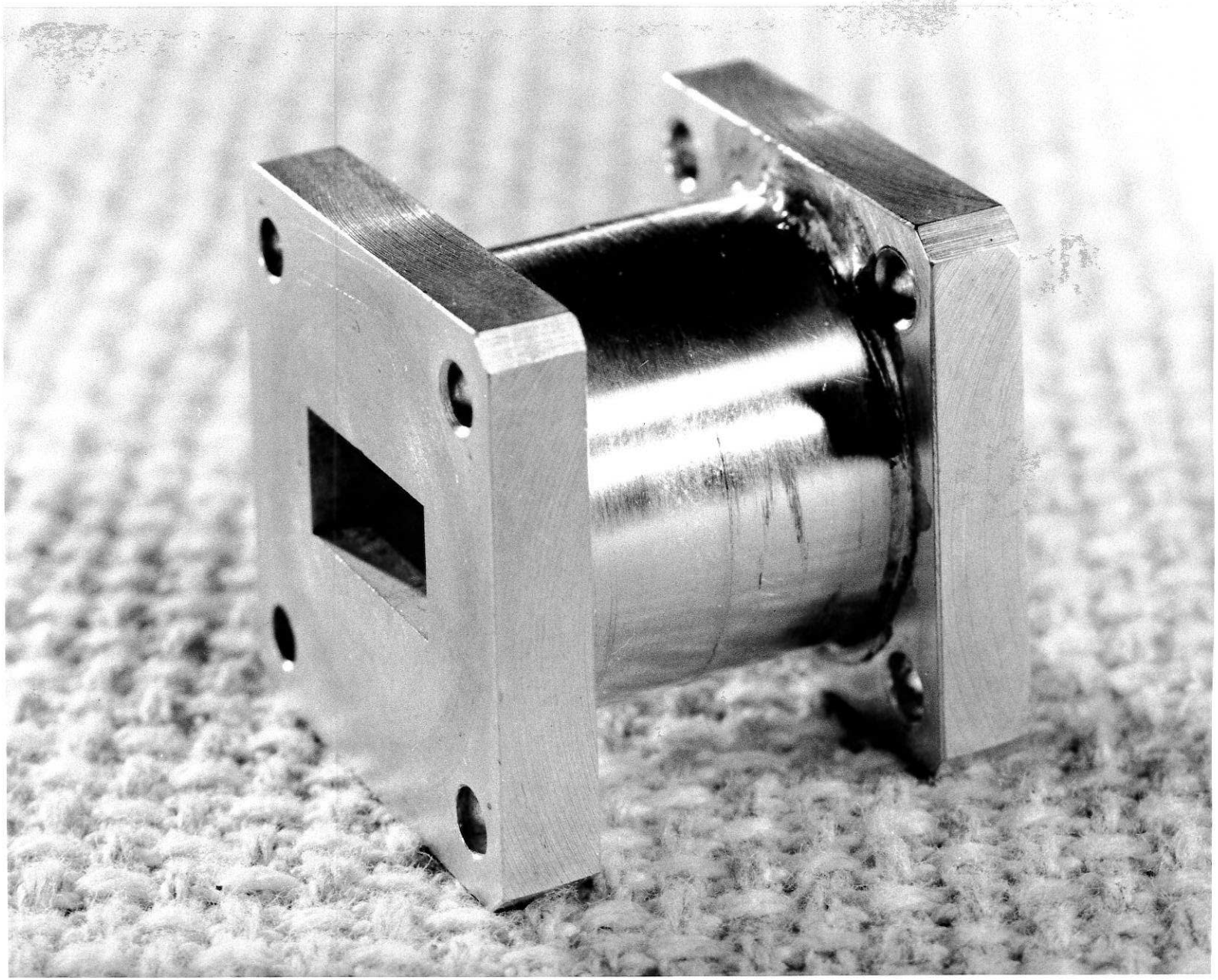

Plate VI — Prototype of ceramic waveguide window

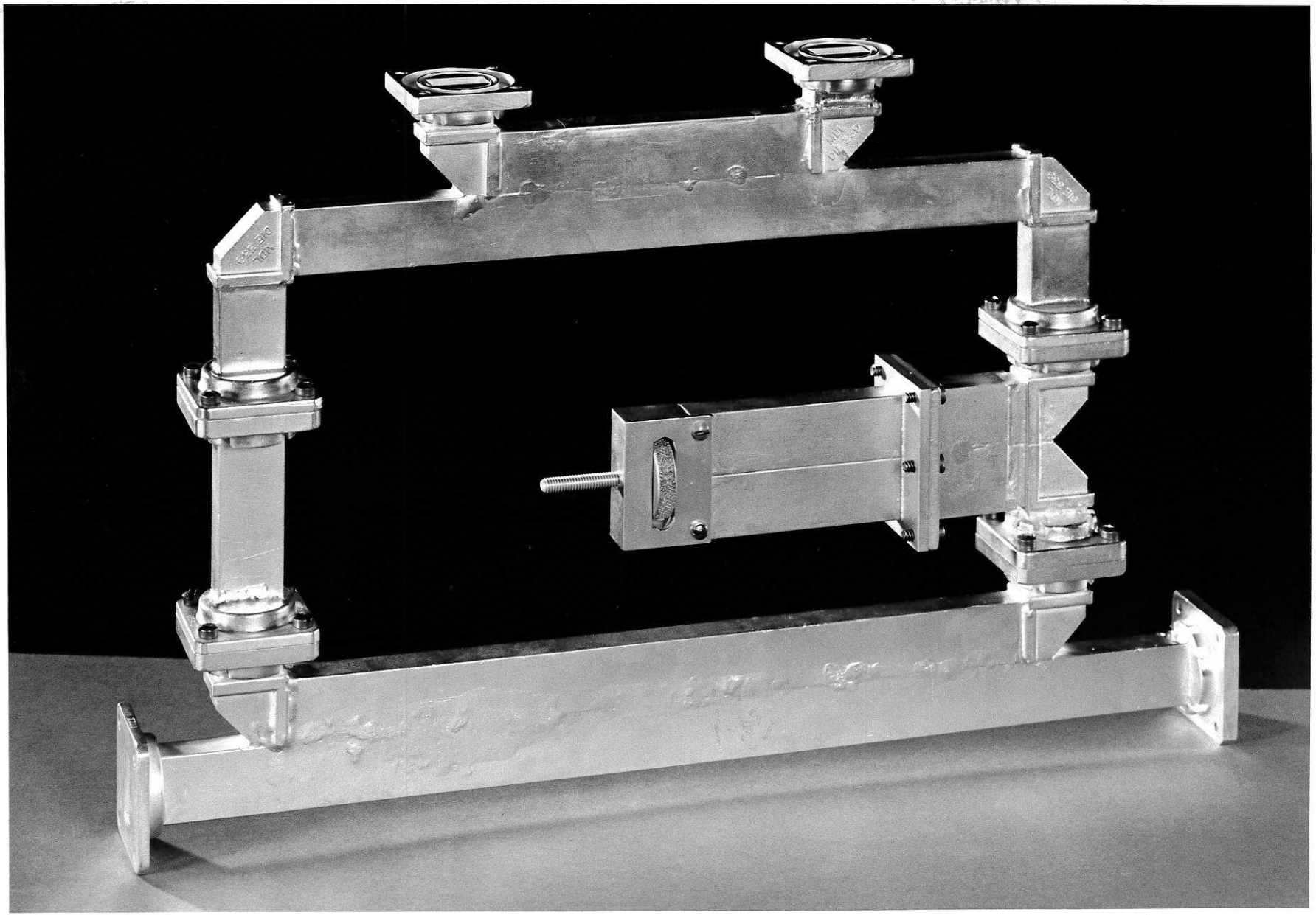

Plate VII — Resonant ring high-power simulator